Available online at www.sciencedirect.com
ScienceDirect
Geochimica et Cosmochimica Acta 71 (2007) 2036–2055
Geochimica et Cosmochimica Acta
www.elsevier.com/locate/gca

Molecular dynamics simulation of the CH_4 and CH_4–H_2O systems up to 10 GPa and 2573 K

Chi Zhang, Zhenhao Duan *, Zhigang Zhang

State Key Laboratory of Lithospheric Evolution, Institute of Geology and Geophysics, Chinese Academy of Sciences, Beijing 100029, China

Received 16 August 2006; accepted in revised form 22 January 2007; available online 26 January 2007

Abstract

Based on our previous study of the intermolecular potential for pure H_2O and the strict evaluation of the competitive potential models for pure CH_4 and the ab initio fitting potential surface across CH_4–H_2O molecules in this study, we carried out more than two thousand molecular dynamics simulations for the *PVTx* properties of pure CH_4 and the CH_4–H_2O mixtures up to 2573 K and 10 GPa. Comparison of 1941 simulations with experimental *PVT* data for pure CH_4 shows an average deviation of 0.96% and a maximum deviation of 2.82%. The comparison of the results of 519 simulations of the mixtures with the experimental measurements reveals that the *PVTx* properties of the CH_4–H_2O mixtures generally agree with the extensive experimental data with an average deviation of 0.83% and 4% in maximum, which is equivalent to the experimental uncertainty. Moreover, the maximum deviation between the experimental data and the simulation results decreases to about 2% as temperature and pressure increase, indicating that the high accuracy of the simulation is well retained in the high temperature and pressure region.

After the validation of the simulation method and the intermolecular potential models, we systematically simulated the *PVTx* properties of this binary system from 673 K and 0.05 GPa to 2573 K and 10 GPa. In order to integrate all the simulation results and the experimental data for the calculation of thermodynamic properties, an equation of state (EOS) is developed for the CH_4–H_2O system covering 673–2573 K and 0.01–10 GPa. Isochores for compositions <4 mol% CH_4 up to 773 K and 600 MPa are also determined in this paper. The program for the EOS can be downloaded from www.geochem-model.org/programs.htm.

1. INTRODUCTION

CH_4-bearing aqueous fluid is one of the most frequently encountered fluids in and around the Earth, occurring in mid-ocean ridge hydrothermal systems (Kelley, 1996), volcanoes (Carroll and Holloway, 1994), fluid inclusions (Mullis et al., 1994), coalfield and oilfield (Roedder, 1979; Kisch and Van Den Kerkhof, 1991; Hedenquist and Lowenstern, 1994; Dubessy et al., 2001) and the methanogenesis in deep aquifers and earth's mantle (Scott et al., 2004; Veto et al., 2004). The *PVTx* (pressure–volume–temperature composition) property is the most fundamental thermodynamic property because it can be used to construct equations of state, which can in turn calculate volumetric properties (density, volume, compressibility, and bulk modulus), phase behaviors (immiscibility, phase equilibrium), heat properties (enthalpy) and chemical properties (activity, fugacity and chemical potential). *PVTx* property is also important in the analysis of fluid inclusions for tracing the formation conditions of geological bodies (Roedder, 1984; Labotka, 1991; Schmidt and Bodnar, 2000) and the study of methane hydrate formation (Sun and Duan, 2005). Nearly one thousand experimental data points (listed in Table 1) have been published for the PVTx properties of the CH_4–H_2O system, but they are limited in their *T* (323.15-7-23.15 K) *P* (0.021–250 MPa) ranges. Lin (2005) successfully extend the *TP* range using synthetic fluid inclusion method to 773 K and 300 MPa, but the experimental

* Corresponding author.
E-mail address: duanzhenhao@yahoo.com (Z. Duan).

0016-7037/$ - see front matter © 2007 Elsevier Ltd. All rights reserved.
doi:10.1016/j.gca.2007.01.017

Table 1
The experimental *PVTx* data of the CH_4–H_2O system

Author	*P* (MPa)	*T* (K)	*X* (H_2O)	Number of points
Welsch (1973)	40–250	648.15–698.15	0–1	Graph
Christotoforakos (1985)	10–100	653.15–673.15	0.1–0.6	Graph
Sretenskaya et al. (1986)	0.1–200	648.15–723.15	0–1	309
Joffrion and Eubank (1988, 1989)	0.021–12.034	323.15–498.15	0.1–0.5	156
Shmonov et al. (1993)	10–200	653–723	0–1	126
Abdulagatov et al. (1993a,b)	2.24–63.24	523.15–653.15	0–1	98
Hnedkovsky et al. (1996)	28–35	298.15–705.45	0.0019–0.0025	31
Fenghour et al. (1996)	7.491–30.382	430–699	0.076–0.6761	87

path to much higher *TP* conditions proves to be very difficult. It seems that alternative approaches must be taken to substantially expand the experimental database and to investigate this binary system in the experimentally difficult *TP* range, so that we will be able to study geochemical processes of the fluid involved in the lower crust and mantle of the Earth.

Recently, molecular level computer simulation (MLCS) emerges as an important new means to study thermodynamic properties in the higher *TP* region. Duan and Zhang (2006) successfully validated the MLCS technique by reproducing thousands of experimental data points for the H_2O–CO_2 system, and extended the experimental database from less than 1000 K and 1 GPa to 2573 K and 10 GPa. The predictability of MLCS has also been demonstrated by many prior workers (Chen et al., 1998; Errington et al., 1998; Birkett and Do, 2004; Konrad and Lankau, 2005; Zhang and Duan, 2005). The success of MLCS, to a large extent, relies on the development of accurate potential models, which can be evaluated from experimental data or from quantum mechanics methods (ab initio etc.). Once the potential model is established, it can be used to predict various thermodynamic, transport and liquid structure properties in a wide *TP* range through MLCS.

In this article, we systematically studied the supercritical *PVTx* properties of the CH_4–H_2O system up to 2573 K and 10 GPa by the MLCS approach as discussed in the article of Duan and Zhang (2006). We begin with a brief introduction of simulation methodology, followed by the choice of the potential model of CH_4–CH_4 molecular interactions and ab initio fitting potential surface between CH_4 and H_2O molecules. Subsequently, MLCS method is validated by comparing all the available experimental data with the simulated results. Based on the valid MLCS method, we predict the *PVTx* property of the CH_4–H_2O system up to 2573 K and 10 GPa and isochors for the CH_4 molar fraction between 0.5% and 4%. Then an equation of state up to 2573 K and 10 GPa is developed based on both the experimental and the simulated data.

2. METHODOLOGY AND SIMULATION DETAILS

In this study, we carried out more than one thousand isothermal–isobaric molecular dynamics simulations with algorithms proposed in our previous paper (Zhang and Duan, 2005). The potential models, simulation algorithms and computational details are briefly described here. The equations below, which was modified by Zhang and Duan (2005) from Martyna et al. (1994), are adopted to propagate the MD trajectories:

$$\ddot{\mathbf{r}}_i = \mathbf{F}_i/m_i + \dot{\eta}^2\mathbf{r}_i + \ddot{\eta}\mathbf{r}_i - (\dot{\xi} + 3\dot{\eta}/f)(\dot{\mathbf{r}}_i - \dot{\eta}\mathbf{r}_i) \tag{1}$$

$$\ddot{\eta} = (P_{\text{inst}} - P_{\text{desire}})\exp(3\eta)/t_p^2 k_B T_{\text{desire}} + \sum_{i=1}^{N} m_i(\mathbf{r}_i - \dot{\eta}\mathbf{r}_i)^2/f t_p^2 k_B T_{\text{desire}} - \xi\dot{\eta} \tag{2}$$

$$\dot{\xi} = \left[\sum_{i=1}^{N} m_i(\dot{\mathbf{r}}_i - \dot{\eta}\mathbf{r}_i)^2 + 3\dot{\eta}^2 t_p^2 k_B T_{\text{desire}} - (f+1)k_B T_{\text{desire}}\right]/Q \tag{3}$$

$$\eta = \ln V^{\frac{1}{3}} \tag{4}$$

$$P_{\text{inst}} = \frac{1}{3V}\sum_{i=1}^{N} m_i(\dot{r}_i - \eta\dot{r}_i)^2 + \frac{W}{V} \tag{5}$$

where r_i, F_i and m_i are the position, force and mass of the i^{th} particle, respectively. ξ and η are the thermostat and barostat variables, with two corresponding parameters of Q and t_p to adjust the fluctuation of temperature and pressure; V is the volume; f is the degree of freedom of the simulated system with N particles; k_B is the Boltzmann constant; P_{desire} and T_{desire} are the desired/external pressure and temperature; P_{inst} is the instantaneous pressure, which is calculated from atomic virial $W = \frac{1}{3}\sum_i F_i \cdot r_i$. According to the suggestion of Martyna et al. (1994),Q and t_p were set with a typical value of 5.0 kJ ps^2/mol and 5.0 ps, respectively, in most cases and NPT ensemble is adopted for the convenience of comparing common experiments. Considering the special needs for the calculation of isochors, t_p was set to infinite and the simulation ensemble turns into NVT in order to obtain fixed volume result.

Cubic boxes, conventional periodic boundary conditions and minimum image conventions were used in all simulations, Eward summation were adopted to calculate the long-range electrostatic forces and energies. The velocity Verlet algorithm, the correction of long-range Lennard–Jones interactions were made with the formulations presented by (Zhang and Duan, 2002). The geometry of the multi-site molecules were restricted by RATTLE method (Andersen, 1983) and O for H_2O and C for CH_4 (five sites model) were chosen for the primary atom in the propagation of MD trajectory. The force acting on other atoms were transformed to the primary atoms as suggested by Ciccotti et al. (2001). Simulations were initialized by "melting" with

the face-centered-cubic lattice structure. The time step were set as 1 fs and the average volume were calculated from the 70 ps statistical average of instantaneous volume after 80 ps pre-equilibrium simulation for most of the simulation. Longer simulations were performed (up to 300 ps after 200 ps in pre-equibrium) in some high pressure zone to ensure the convergence of the simulation. The finite-size effect was carefully checked and only insignificant changes were found when the system increases from 256 to 512 molecules. Our simulations were carried out with at least 300 molecules. In order to compare with experimental data of the binary mixtures, the total number of molecules is adjusted between 300 and 512 to precisely pinpoint the corresponding experimental composition within 0.03‰.

3. INTERACTION POTENTIALS

Accurate description of intermolecular potential plays the key role in the success of molecular simulation. The intermolecular potential is often characterized as functions of molecular distance, charges etc. One of the most widely used forms is 12-6 Lennard–Jones (LJ) potential with the additional Coulomb interactions:

$$U_{ij} = \sum_i \sum_j 4\varepsilon_{ij}\left[\left(\frac{\sigma_{ij}}{r_{ij}}\right)^{12} - \left(\frac{\sigma_{ij}}{r_{ij}}\right)^{6}\right] + \sum_i \sum_j \frac{q_i q_j}{r_{ij}} \qquad (6)$$

where U_{ij} is the potential energy, r_{ij} is the distance between two interaction sites i and j, q_i and q_j are the partial charges designated on the interaction sites, ε_{ij} and σ_{ij} are the adjustable parameters for the Lennard–Jones potential.

Another formula for molecular potential is the EXP6 form:

$$U_{ij} = \varepsilon_{ij}\left\{\frac{6}{\alpha_{ij}-6}\exp\left[\alpha_{ij}\left(1-\frac{r_{ij}}{r^*_{ij}}\right)\right] - \frac{\alpha_{ij}}{\alpha_{ij}-6}\left(\frac{r^*_{ij}}{r_{ij}}\right)^6\right\} + \sum_i \sum_j \frac{q_i q_j}{r_{ij}} \qquad (7)$$

where r^*_{ij} refers to the position of the minimum and αij and ε_{ij} are the adjustable parameters and the other definitions are the same with the LJ potential.

There are three kinds of molecular interactions involved in the CH_4–H_2O system: H_2O–H_2O, CH_4–CH_4 and CH_4–H_2O interactions. We have extensively searched for H_2O–H_2O potential and the SPC/E potential was found to accurately predict PVT properties of water at least up to 5 GPa and possibly up to 20 GPa (Zhang and Duan, 2005). Therefore, we only need to investigate the CH_4–CH_4 and CH_4–H_2O potential in this study.

3.1. CH_4–CH_4 potential

Many molecular potential models have been proposed for the investigation of the thermodynamic properties of CH_4 (Williams, 1967; Fitzwater and Bartell, 1976; Murad and Gubbins, 1978; Righini et al., 1981; Meinander and Tabisz, 1983; Jorgensen et al., 1984; Schoen et al., 1986; Saager and Fischer, 1990; Schindler et al., 1993; Kaminski et al., 1994; Nagy et al., 1995; Errington et al., 1998). Stassen (1999) reviewed the performance of most of the potential models and found that the simple one site LJ model played the best in the PVT property predictions. However, his comparison was only made at a single point of $T = 150$ K, $P = 103.85$ MPa. A comprehensive evaluation in a wide TP range is necessary in order to find the transferability and predictability of a model. Birkett and Do (2004) examined the PVT properties of a newly developed one site EXP6 potential optimized by Errington et al. (1998) for phase equilibrium and the result is generally good. The one site LJ OPLS potential (Jorgensen et al., 1984), one site EXP6 potential (Errington et al., 1998) and the more complicated five sites OPLS-SITE potential (Kaminski et al., 1994), which claims to improve the structure performance of OPLS, are selected as the most competitive candidates for the final choice in the study of pure CH_4. A large number (1941 points) of molecular dynamic simulations of PVT property were carried out in this study to compare with experimental data and to verify the validity of these three interaction potentials in the high TP region. The parameters of the potential models used in this study are listed in Table 2. As we will discuss in Section 4, the OPLS potential most accurately reproduces the experimental data of the 1941 points with an average error of 0.96%.

Table 2
Molecular potential models of CH_4

Model	Potential Type	Reference	Parameters	
OPLS	1c LJ	Jorgensen et al. (1984)		$\sigma = 3.73\times10^{-10}$ m $\varepsilon/k_B = 147.94$ K
OPLS-SITE	5c LJ + Coulomb	Kaminski et al. (1994)	C–C:	$\sigma = 3.50\times10^{-10}$ m $\varepsilon/k_B = 33.21$ K
			C–H:	$\sigma = 3.00\times10^{-10}$ m $\varepsilon/k_B = 22.39$ K
			H–H:	$\sigma = 2.50\times10^{-10}$ m $\varepsilon/k_B = 15.10$ K
			Configuration:	$d_{CH} = 1.09\times10^{-10}$ m $q_C = -4q_H = -0.24$ e
MEXP6	1c EXP6	Errington et al. (1998)		$\sigma = 3.741\times10^{-10}$ m $\varepsilon/k_B = 160.3$ K $\alpha = 15$

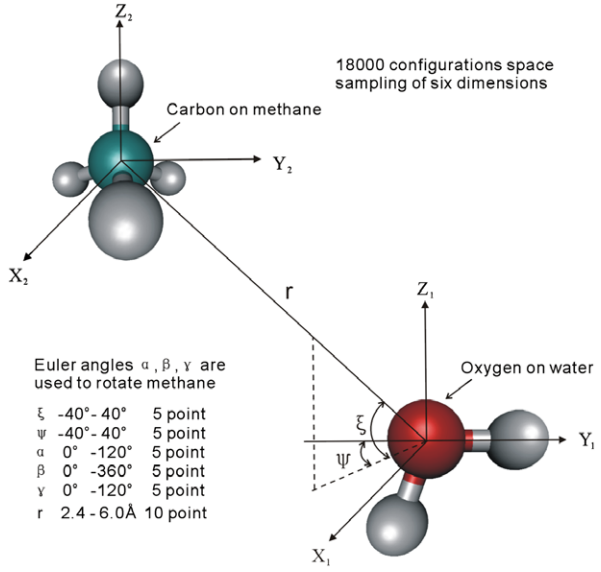

Fig. 1. The CH_4–H_2O inter-molecular structure in quantum calculations (Cao et al., 2001).

3.2. CH_4–H_2O potential

The CH_4–H_2O potential can be obtained directly from mixing the H_2O–H_2O parameters and CH_4–CH_4 parameters with combining rules. The Lorentz–Berthelot (LB) combining rule is the most simple and widely used one:

$$\varepsilon_{ij} = \sqrt{\varepsilon_i \varepsilon_j} \tag{8}$$

$$\sigma_{ij} = (\sigma_i + \sigma_j)/2 \tag{9}$$

The Kong combining rule, which considered superior for accurate predictions of equilibrium properties, is also tested in this study:

$$\varepsilon_{ij}\sigma_{ij}^{12} = (\varepsilon_{ii}\sigma_{ii}^{12}/2^{13})[1 + (\varepsilon_{jj}\sigma_{jj}^{12}/\varepsilon_{ii}\sigma_{ii}^{12})^{1/13}]^{13} \tag{10}$$

$$\varepsilon_{ij}\sigma_{ij}^{6} = (\varepsilon_{ii}\sigma_{ii}^{6}\varepsilon_{jj}\sigma_{jj}^{6})^{1/2} \tag{11}$$

Duan and Zhang (2006) investigated the two combining rules above and found that they cannot accurately yield mixing properties. However, the interaction potential obtained from ab initio results give much more accurate predictions than the traditional combining rules. In this study, we again investigated the predictability of the three kinds of cross molecule interactions for the CH_4–H_2O system.

The quantum based potential surface has been calculated by several research groups (Szczesniak et al., 1993; Cao et al., 2001; Klauda and Sandler, 2002). In this study, we used the latest ab initio result calculated by Cao et al. (2001). The interaction energies were firstly calculated by MP2 methods with 6-31++G(2d,2p) basis set on all 18,000 points with different six dimensions $r, \xi, \phi, \alpha, \beta, \gamma$ as shown in Fig. 1, then corrected with ~100 MP2/cc-pVQZ results to minimizing basis set superposition error. The method were thought to achieve nearly MP2/cc-pVQZ accuracy for all 18,000 points.

We could use atomic site–site potential model for the interactions between CH_4 and H_2O molecules so that the angle-dependence can be taken into account. However, we have to adopt Boltzmann-weighted average to fit a spherically symmetric radial potential with the ab initio results, because the five site OPLS model for CH_4 is much less accurate than the spherical one-site OPLS model as discussed below, and the rapid molecular movement under high temperatures averaged the angle-dependence. The average potential energy at each distance are calculated using the following equation and then fitted to an LJ form

$$\langle E_{\mathrm{rp}}(r)\rangle = \frac{\sum E_{\mathrm{i}}(r)\exp(-E_{\mathrm{i}}(r)/k_{\mathrm{B}}T)}{\sum \exp(-E_{\mathrm{i}}(r)/k_{\mathrm{B}}T)} \tag{12}$$

where k_B is the Boltzmann constant, r represents the C–O distance, T is the absolute temperature, E_i stands for the configuration potential and E_{rp} for the calculated potential. Temperature is a very important factor in the Boltzmann averaging calculations. It is known that the Boltzmann-average energy ascends when the temperature increases but we found that the mean potential energy does not change significantly for temperature above 273 K and the simulation results are not sensitive to the choice of temperature in our practice. Therefore, we chose the temperature at 1073 K as a reference since it is in the middle of the temperature range of our interests. Considering the potential energy at $r = 2.4 \times 10^{-10}$ m is nearly one order of magnitude lager than the other nine and is also less accurate as noted by Cao et al. (2001), its not include in the fitting procedure. The final fitted parameters are $\sigma = 3.317 \times 10^{-10}$ m, $\varepsilon/k_B = 113.58$ K. As shown below, this approach works efficiently for this binary system above 323 K. It is found that the distance of potential well in this parameterized potential are $\sqrt[6]{2}\sigma = 3.723 \times 10^{-10}$ m, which is near the experimental center-of-mass distance 3.70×10^{-10} m between methane and water at ground state from far infrared vibration-rotation-tunneling spectroscopy (Dore et al., 1994).

4. SIMULATION RESULTS AND DISCUSSION

4.1. Pure CH_4

For the *PVT* property of CH_4, Grevel (1993) found more than 6000 experiments data points covering a *TP* range from 91.15 to 723 K and from 0.021 to 1015.5 MPa. In this study, the relatively high temperature data (above 273 K) and the lately publish results (listed in Table 3) are used to examine the veracity of the MLCS in the range of 273.15–723 K and 0.5–1015.5 MPa. The shock-wave data up to 6528 K, 119.6 GPa, reported by Ross and Ree (1980), are taken as an identifier of the transferability and predictability of the MLCS method in the ultrahigh *TP* region.

Robertso and Babb (1969) measured the isotherms of CH_4 up to 1005.5 MPa, which is the highest experimental pressure reported until now. Fig. 2 shows the deviation between MLCS results and experiment, displaying that the accuracy of MLCS relies on the choice of the different potential models. The OPLS model demonstrates an excellent predictability with a maximum deviation less than 1%, and an average of 0.11% from experimental data. The EXP6

Table 3
The Experimental *PVT* data of CH_4

Author	*P* (MPa)	*T* (k)	No	Remarks
Michels and Nederbragt (1935)	1.9–8.2	273.15–423.15	56	(2) (3)
Michels and Nederbragt (1936)	1.9–38.9	273.15–423.15	119	(1) (2) (3)
Olds et al. (1943)	1.4–69.0	294.15–511.15	280	(1) (3)
Schamp et al. (1958)	1.8–26.1	273.15–423.15	118	(1) (3)
Deffet et al. (1964)	1.0–304.0	324.15–425.15	228	(1) (3)
Douslin et al. (1964)	1.6–40.6	273.15–623.15	374	(1) (2) (3)
Robertso and Babb (1969)	150.4–1015.5	302.15–473.15	108	(1) (3)
Tsiklis et al. (1971)	202.7–861.3	323.15–573.15	70	(1)
Trappeniers et al. (1979)	1.8–259.4	273.15–423.15	472	(2)
Ross and Ree (1980)	1900–119,600	384–6528	8	(4)
Achtermann et al. (1986)	5.0	11–287	35	
Shmonov et al. (1993)	10–200	653.–723	21	(5)
Abdulagatov et al. (1993b)	3.92-58.86	523.15-653.15	17	
Abdulagatov et al. (1996)	0.5–95.6	523.15–673.15	47	

(1) Data used for fitting Duan's equation (Duan et al., 1992a).
(2) Data used by IUPAC data (Angus et al., 1978).
(3) Data used for fitting the modified Redlich–Kwong equation (Grevel, 1993).
(4) Shockwave data.
(5) Four data points show significant deviation from other data sets, suggesting a misprint of the reported value. These data are not used in this study.

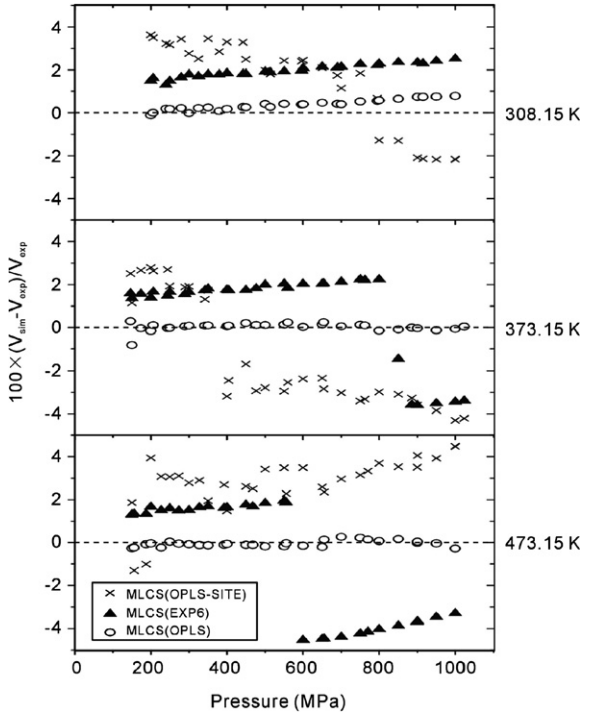

Fig. 2. Comparison of the molecular simulation results with the data of Robertso and Babb (1969).

and OPLS-SITE potential models, however, yield much larger maximum deviations of 4.53% and 4.83%, respectively. In the high pressure region, the OPLS model gives improving accuracy as temperature increases with the maximum deviations of 0.43% and 0.21% at 373.15 K and 473.15 K, respectively.

Fig. 3 displays the comparison of the simulation results with the most recently published high temperature data of Abdulagatov et al. (1996) (note that the OPLS-SITE results with error bigger than 3% were not shown in the figure for clarity). The performances of the molecular simulation with both OPLS and EXP6 potential model are quite similar in the relatively lower *TP* region where the maximum deviation is below 1%. However, as the temperature and pressure increase, the deviation between the results derived from EXP6 potential model and experiment becomes significant, reaching 2.63% at the point $T = 648.15$ K and $P = 91.281$ MPa. The OPLS potential again shows quite stable predictability in the whole *TP* region where the average error is 0.23% and the maximum is 1.06%.

Similarly, the simulation results with OPLS potential agree well with the 1941 *TP* experimental points; the average deviation is 0.96% and the maximum deviation is

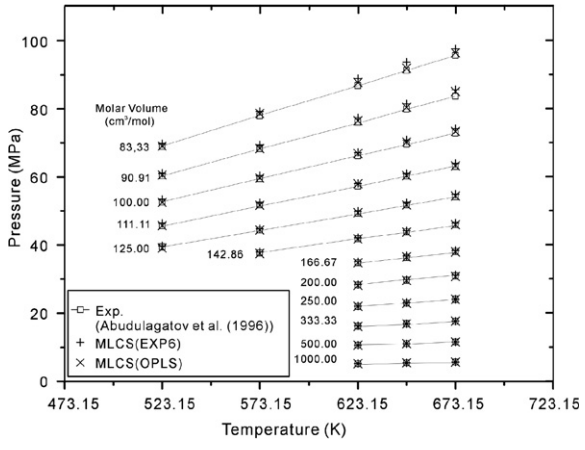

Fig. 3. Comparison of the simulation results with the data of Abdulagatov et al. (1996).

2.82%. On the other hand, the EXP6 and OPLS-SITE potentials, yield much larger average deviations of 2.3% and 4.0%, respectively. The successful reproduction of all experiment data in a wide *TP* range with the OPLS potential model convinces us that the method and potential should have much better predictability than other models.

The shockwave data (Ross and Ree, 1980) are used to estimate the predictability of MLCS in the very high pressure region. The results of different potential models are listed in Table 4. Again the OPLS potential shows great predictability with the deviation below 1.29% up to $T = 1912$ K and $P = 15.9$ GPa. By contrast, the simulation results with the EXP6 and the OPLS-SITE potentials yield much larger deviations of 5.24% and 19.59%, respectively. In ultra high *TP* region ($T \geqslant 3268$ K, $P \geqslant 29{,}400$ MPa), the simulation with all potentials yields larger volume than shockwave data by more than 5%. This might be the valid upper limit of our simulation.

Strauss et al. (1996) obtained the liquid structure of CD_4 from neutron diffraction and use the reverse Monte Carlo technique to evaluate a pair potential model for liquid CD_4. As shown in Table 5, all potential model shows quit good agreement with experiments in peak positions, but the peak heights vary.

Table 4
The molecular simulation (MS) results of CH_4 as compared with shockwave data

T (K)	*P* (MPa)	Molar volume (cm^3/mol)			
		Experiment	MS (OPLS)	MS (OPLS-site)	MS (EXP6)
384	1900	25	24.85	25.46	24.87
728	4600	21.68	21.63	23.2999	22.01
1912	15900	17	17.22	20.33	17.89
3268	29400	14.9	15.93	—	16.01
6528	60000	12.7	14.40	—	14.43
3626	62200	12	13.63	—	13.29
3906	84400	11	12.78	—	12.35
4438	119600	9.97	11.91	—	11.37

4.2. Pure H_2O

Zhang and Duan (2005) systematically performed a series of isothermal–isobaric molecular dynamics simulations over a wide range of temperatures and pressures to evaluate the PVT properties of water with SPC/E potential. Compared with the most recent published high-pressure experimental data up to 5.0 GPa, the simulation results with SPCE show remarkable agreement with errors less than 1.0%. Considering this potential was proposed based on only a few experimental data under room temperatures and pressures, the high accuracy of the simulation results indicate a great predictive power of molecular level study and verify our attempt of using molecular dynamics simulations to generate data as an important supplement to the database of experimental properties of geological fluids. Besides PVT properties, Wasserman et al. (1995) studied the dielectric constants up to 5000 bar and 823 K, which is also consistent with experimental data. Boulougouris et al. (1998) evaluated the enthalpy of vaporization from 300 to 600 K, $g(r)$ at 298 and 523 K, which shows general consistence between experiments and the simulated results. SPC/E cannot reproduce gas phase (or low density phase) properties, including single molecule dipole moment.

4.3. CH_4–H_2O binary

All the experimental data in Table 1 are projected onto Fig. 4, showing the *TP* range of the existing experiment data. These data can be divided into two portions: one is below 648.15 K with pressures below 50 MPa, and the other is between 648 and 723 K with pressures up to 250 MPa. We carried out 519 simulations corresponding to the experimental conditions in order to find out the accuracy and the predictability of the MLCS method.

In the high-pressure portion, Welsch (1973) measured the *PVTX* data of CH_4–H_2O system with the *TP* range of $648.15 \leqslant T \leqslant 698.15$ K, $40 \leqslant P \leqslant 250$ MPa. Sretenskaya et al. (1986) and Shmonov et al. (1993) reported experimental data covering nearly the same region but found to be inconsistent with Welsch (Grevel, 1993; Shmonov et al.,

Table 5
Maxima/minima positions (10^{-10} m) and heights of $g_{CC}(r)$ for CH_4: MD *vs.* experiment

Model	First max/heights	First min/heights	Second max/heights	Second min/heights	
OPLS	4.1/2.86	5.7/0.60	7.7/1.27	9.4/0.84	150 K, 0.449 g/cm^3
OPLS-site[a]	4.1/2.39	5.7/0.63	7.8/1.17	9.3/0.85	150 K, 0.449 g/cm^3
EXP6	4.1/2.95	5.7/0.56	7.7/1.29	9.4/0.81	150 K, 0.449 g/cm^3
Exp[a,b]	4.1/2.13	5.8/0.65	7.9/1.13	9.5/0.87	150 K, 0.449 g/cm^3
OPLS	3.9/1.65	6.5/0.90	8.0/1.04		370 K, 0.27 g/cm^3
Exp[b]	3.9/1.45	6.5/0.94	8.0/1.06		370 K, 0.27 g/cm^3
OPLS	3.9/1.70	6.4/0.89	8.0/1.03		370 K, 0.31 g/cm^3
Exp[b]	3.9/1.46	6.4/0.92	7.9/1.05		370 K, 0.31 g/cm^3
OPLS	3.9/1.75	6.3/0.87	8.0/1.02		370 K, 0.34 g/cm^3
Exp[b]	3.9/1.48	6.5/0.91	7.8/1.05		370 K, 0.34 g/cm^3

[a] Data from Stassen (1999), model C in his Table 3.
[b] Obtained from the potential model adjusted from neutron diffraction data on CD4 by reverse Monte Carlo simulation (Strauss et al., 1996).

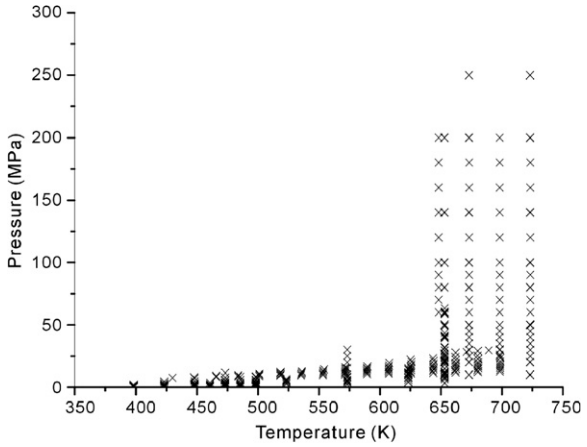

Fig. 4. The distribution of experimental $PVTx$ data of the CH_4–H_2O system in TP space.

1993). Fig. 5 compares all three experimental data sets, showing that the data of Welsch deviate substantially from those of Sretenskaya et al. (1986) and Shmonov et al. (1993). This may be resulted from Welsch's inaccurate pressure and composition measurements as pointed out by Shmonov et al. (1993). We, therefore, only compare our simulation results with the other two data sets (Tables 6 and 7).

Among the three CH_4–H_2O potential models obtained from the Lorentz-Bethelot combining rule (LB), Kong combining rule (Kong) and fitting ab initio quantum calculated results (ab initio), the ab initio potential yields the best predictions, especially in the water rich samples. The simulated volume deviates from that of Shmonov et al. (1993) by 0.53% on average and 2.40% in maximum. The performances of the LB and Kong potential are much worse and the deviations reach 5.2% and 5.89%, respectively. Similar results are observed in the comparisons with the data of Sretenskaya et al. (1986). The ab initio potential yields an average deviation of 0.58%, but the other two potential models have an average deviation of 1.38% and 1.83%, respectively. Since the simulation results with the potential obtained from the LB and Kong combining rules yield similar results, we will not discuss Kong combining rule.

Excess volume, as defined below, is a measure of the non-ideality of fluid mixing and therefore experimental data of excess volume provide another test for the MLCS results.

$$V_{\text{excess}} = V_{\text{mixture}} - x_{CH_4} V_{CH_4} - x_{H_2O} V_{H_2O} \tag{13}$$

$$\sigma_{\text{excess}} = \sqrt{\sigma^2_{\text{mixture}} + x_{CH_4}\sigma^2_{CH_4} + x_{H_2O}\sigma^2_{H_2O}} \tag{14}$$

where V_{excess} is the calculated excess volume, V_{mixture} is the molar volume of the mixture, x_{CH_4} is the mole fraction of methane, V_{CH_4} and V_{H_2O} are molar volumes of pure methane and water at the same TP condition. σ_{excess}, σ_{mixture}, σ_{CH_4} and σ_{H_2O} represents the uncertainty of V_{excess}, V_{mixture}, V_{CH_4} and V_{H_2O}, respectively.

As shown in Fig. 6, the experimental excess volume (Sretenskaya et al., 1986; Shmonov et al., 1993) are well predicted by our simulation, and they fall into the error bar of MLCS results with the ab initio potential. The deviation between simulation and experiment decreases as pressure increases, indicating that the MLCS method can be extrapolated to higher TP region, where there is no experimental data.

In the lower pressure portion, Joffrion and Eubank (1988, 1989) reported accurate $PVTx$ measurements for 10, 25, and 50 mole % of water in the binary system using a Burnett–lsochoric (B–I) apparatus. The effects of H_2O adsorption on the measured pressures was corrected using a Brunauer–Emmett–Teller (BET) adsorption model with applicable BET adsorption constants. Fig. 7 shows the comparison between our simulation and their experimental isochores. The simulated results with the LB combining rule and ab initio fitting potential are generally 2–4% higher than the experimental pressure. As pressure increases, the deviations between ab initio fitting potential results and experimental data are reduced to less than 2%. For the

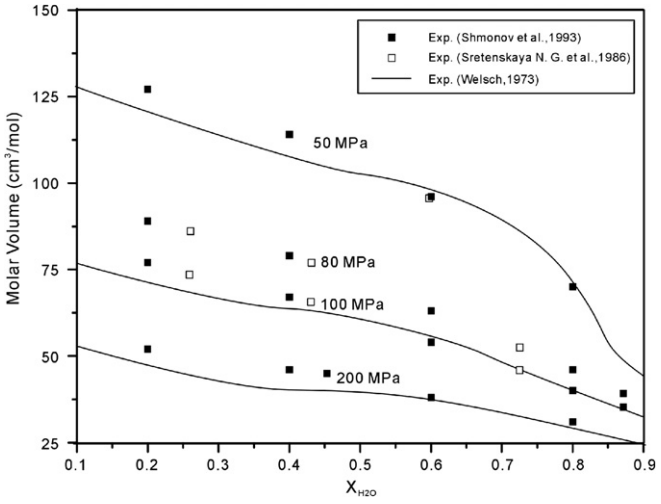

Fig. 5. The inconsistency of different experiment data sets for the CH_4–H_2O mixtures at 673.15 K.

Table 6
Molecular simulation results of the CH_4–H_2O mixtures as compared with the experimental data of Shmonov et al. (1993)

X_{H_2O}	T (K)	P (MPa)	Molar volume (cm^3/mol)						
			Exp.	MLCS (ab initio)	Dev. (%)	MLCS (LB)	Dev. (%)	MLCS (Kong)	Dev. (%)
0.2	673	50	127	125.5994	−1.10	128.7052	1.34	129.4882	1.96
0.4	673	50	114	112.5942	−1.23	115.4101	1.24	115.8363	1.61
0.6	673	50	96	93.7878	−2.30	95.516	−0.50	96.7465	0.78
0.8	673	50	70	68.3231	**−2.40**	67.5834	−3.45	66.3432	−5.22
0.2	673	80	89	88.2693	−0.82	89.1795	0.20	90.4215	1.60
0.4	673	80	79	77.9129	−1.38	78.9718	−0.04	78.7603	−0.30
0.6	673	80	63	63.1041	0.17	64.382	2.19	65.3768	3.77
0.8	673	80	46	45.5927	−0.89	46.912	1.98	47.2706	2.76
0.2	673	100	77	76.0672	−1.21	77.0412	0.05	77.6232	0.81
0.4	673	100	67	66.5989	−0.60	67.6838	1.02	68.3936	2.08
0.6	673	100	54	54.1407	0.26	55.7432	3.23	55.9995	3.70
0.8	673	100	40	40.5202	1.30	41.2596	3.15	41.8803	4.70
0.2	673	200	52	51.8923	−0.21	52.8112	1.56	52.9746	1.87
0.4	673	200	46	45.4789	−1.13	46.388	0.84	46.5473	1.19
0.6	673	200	38	38.0226	0.06	39.1451	3.01	39.5419	4.06
0.8	673	200	31	30.2737	−2.34	31.3648	1.18	31.2887	0.93
0.2	723	50	140	139.1761	−0.59	137.5435	−1.75	138.9408	−0.76
0.4	723	50	127	127.4839	0.38	129.0663	1.63	127.2875	0.23
0.6	723	50	111	108.5015	−2.25	107.7662	−2.91	109.1605	−1.66
0.8	723	50	88	87.3778	−0.71	90.6343	2.99	82.819	**−5.89**
0.2	723	80	95	94.789	−0.22	96.3685	1.44	96.6461	1.73
0.4	723	80	86	84.6566	−1.56	86.7458	0.87	86.8984	1.04
0.6	723	80	71	70.6466	−0.50	72.5737	2.22	73.4671	3.47
0.8	723	80	53	52.8626	−0.26	54.9098	3.60	55.1909	4.13
0.2	723	100	81	80.2218	−0.96	81.333	0.41	83.0351	2.51
0.4	723	100	72	72.086	0.12	73.2617	1.75	73.8677	2.59
0.6	723	100	61	60.6532	−0.57	61.4736	0.78	61.9522	1.56
0.8	723	100	46	46.1496	0.33	46.8464	1.84	47.1368	2.47
0.2	723	200	54	54.3456	0.64	55.1225	2.08	55.4118	2.61
0.4	723	200	48	47.9405	−0.12	48.8866	1.85	49.2024	2.50
0.6	723	200	40	40.6141	1.54	41.5254	3.81	42.0148	5.04
0.8	723	200	32	32.5006	1.56	33.6634	**5.20**	33.8131	5.67
Average deviation (%):					−0.53%		1.34%		1.67%

LB combining rule, however, the deviation has a maximum error of 5.67%.

The densities of CH_4–H_2O mixtures in the temperature range 433–699 K and the pressure range from 7.5 to 30 MPa are measured by Fenghour et al. (1996) using fully automated isochoric instrument. These data are compared with our simulation results with the ab initio potential and the LB potential, as shown by Fig. 8. The ab initio potential model yields the molar volume data consistent with the experimental results with a maximum deviation of 4% and an average deviation of 0.83%. However, results from LB combining rule deviate from experimental data by as much as 7.27%. We noticed that most of the larger deviations for both interaction potentials are found at temperatures close to the critical temperature of water, and this coincides with the difficulty of SPC/E model near the critical region (Zhang and Duan, 2005).

Fig. 9 comprehensively compared all the experimental data mentioned above with our MLCS results with the ab initio potential. It is remarkable that all the data are well reproduced with a maximum deviation of about 4%. It is interesting to note that the deviations between the simulated and experimental values decrease as pressure increases. When the pressure increases above 100 MPa, the simulation results are within about 2% of experimental values, which are equivalent to experimental error.

5. PREDICTION OF PVT_X PROPERTIES

5.1. PVT_x properties beyond the experimental data range

The objective of this study is not only to reproduce the existing experimental data or interpolate between data points in the $PVTx$ space, but also, more importantly, to predict properties in the $PVTx$ space where there is little or no experimental data. We and many others (Belonoshko and Saxena, 1991; Birkett and Do, 2004; Duan and Zhang, 2006) have shown the predictability of MLCS for such fluids as H_2O and H_2O–CO_2 mixtures. As discussed above, in this study more than two thousand of simulations were per-

Table 7
Molecular simulation results of the CH_4–H_2O mixtures as compared with experimental results of Sretenskaya et al. (1986)

X_{H_2O}	T (K)	P (MPa)	Molar volume (cm^3/mol)						
			Exp.	MLCS (ab initio)	Dev. (%)	MLCS (LB)	Dev. (%)	MLCS (Kong)	Dev. (%)
0.5975	673.15	50	95.59	92.7285	−2.99	94.6412	−0.99	95.0353	−0.58
0.2607	673.15	80	86.08	85.7322	−0.40	87.4016	1.54	87.3929	1.53
0.4314	673.15	80	76.91	75.292	−2.10	76.8072	−0.13	77.0814	0.22
0.7252	673.15	80	52.4	52.3427	−0.11	53.8232	2.72	54.2283	3.49
0.8715	673.15	80	39.2	39.28	0.20	40.4012	3.06	40.5492	3.44
0.2591	673.15	100	73.46	73.9159	0.62	74.6393	1.61	74.8683	1.92
0.4304	673.15	100	65.57	64.8709	−1.07	65.9963	0.65	66.4986	1.42
0.7249	673.15	100	45.91	45.8805	−0.06	47.0289	2.44	47.6925	**3.88**
0.8714	673.15	100	35.23	35.4916	0.74	36.4034	**3.33**	36.3121	3.07
0.4530	673.15	200	44.94	43.9904	−2.11	44.7034	−0.53	44.7576	−0.41
0.8861	673.15	200	27.07	27.069	0.00	27.7486	2.51	28.0355	3.57
0.3112	723.15	50	129.8	131.5977	1.38	133.1545	2.58	131.8816	1.60
0.5975	723.15	50	107.8	107.4925	−0.29	109.1311	1.23	108.9117	1.03
0.8652	723.15	50	72.75	70.6908	−2.83	71.5697	−1.62	72.8102	0.08
0.2607	723.15	80	92.3	92.1018	−0.21	93.7022	1.52	93.71	1.53
0.4314	723.15	80	83.66	82.7173	−1.13	83.9105	0.30	84.9299	1.52
0.5708	723.15	80	73.74	73.355	−0.52	74.3966	0.89	74.8972	1.57
0.2591	723.15	100	79.36	79.2847	−0.09	79.8321	0.59	79.9234	0.71
0.4304	723.15	100	70.93	70.3562	−0.81	71.9264	1.40	72.3071	1.94
0.7249	723.15	100	51.8	51.7437	−0.11	52.7735	1.88	53.3276	2.95
0.8714	723.15	100	40	40.0727	0.18	41.1163	2.79	41.435	3.59
0.4530	723.15	200	47.34	46.2622	−2.28	47.164	−0.37	47.546	0.44
0.8861	723.15	200	28.91	29.1202	0.73	29.8142	3.13	29.9733	3.68
Average Deviation(%):					−0.58%		1.38%		1.83%

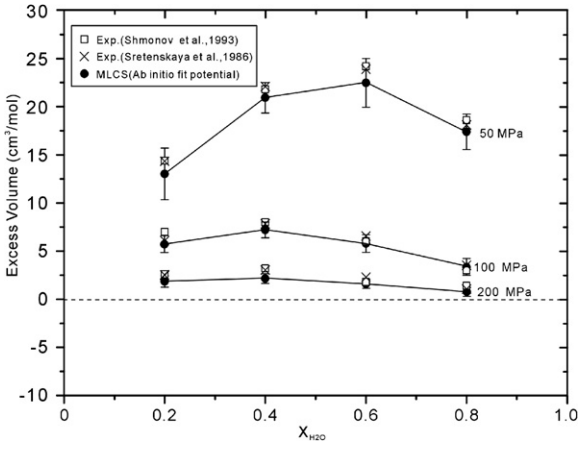

Fig. 6. Comparison of the MLCS simulated excess volume and experimental data.

formed and the MLCS results agree remarkably well with experimental values. Especially, as temperature and pressure increase, the accuracy increases, suggesting that the MLCS method can be adopted to study the $PVTx$ properties beyond current experimental range.

As shown above, accurate description of the $PVTx$ mainly depends on the character of potential model. The OPLS potential we used to model CH_4–CH_4 molecular interaction provides good agreement with experimental data up to $T = 3268$ K, $P = 29.4$ GPa. The SPC/E potential we used to model the H_2O–H_2O molecular interaction also produces good agreement with experimental data up to $T = 1373.15$ K and $P = 5$ GPa and can even be reliably extended to extend to the higher TP region (Zhang and Duan, 2005). Though the ab initio fit potential we used to model the CH_4–H_2O molecular interaction cannot be tested in the higher TP region due to the lack of data, the success for the end-members (CH_4 and H_2O) and for the CH_4–H_2O mixtures, where data are available, convinced us that we should be able to predict the binary mixture properties up to very high TP range. We, therefore, extend our simulation to predict the $PVTx$ properties up to 2573 K and 10 GPa (Table 8), with the largest uncertainties less than 4%, when compared with available experimental data, and the average error in density should be less than 2%. These results should be treated as virtual state of measurements where no chemical reactions are taken into account and they are important supplement to the experiments.

5.2. Isochore for fluid inclusions

In Fig. 10, we calculated the isochores employing NVT molecular dynamic simulation. The homogenization curves and molar volume are calculated using the equation of state proposed by Duan et al. (1992b). At each homogenization point, constant volume simulation is carried out at 673.15 and 773.15 K. Linear fit (including homogenization points) is then taken to give a prediction of the isochores. The iso–Th curves reported by Lin

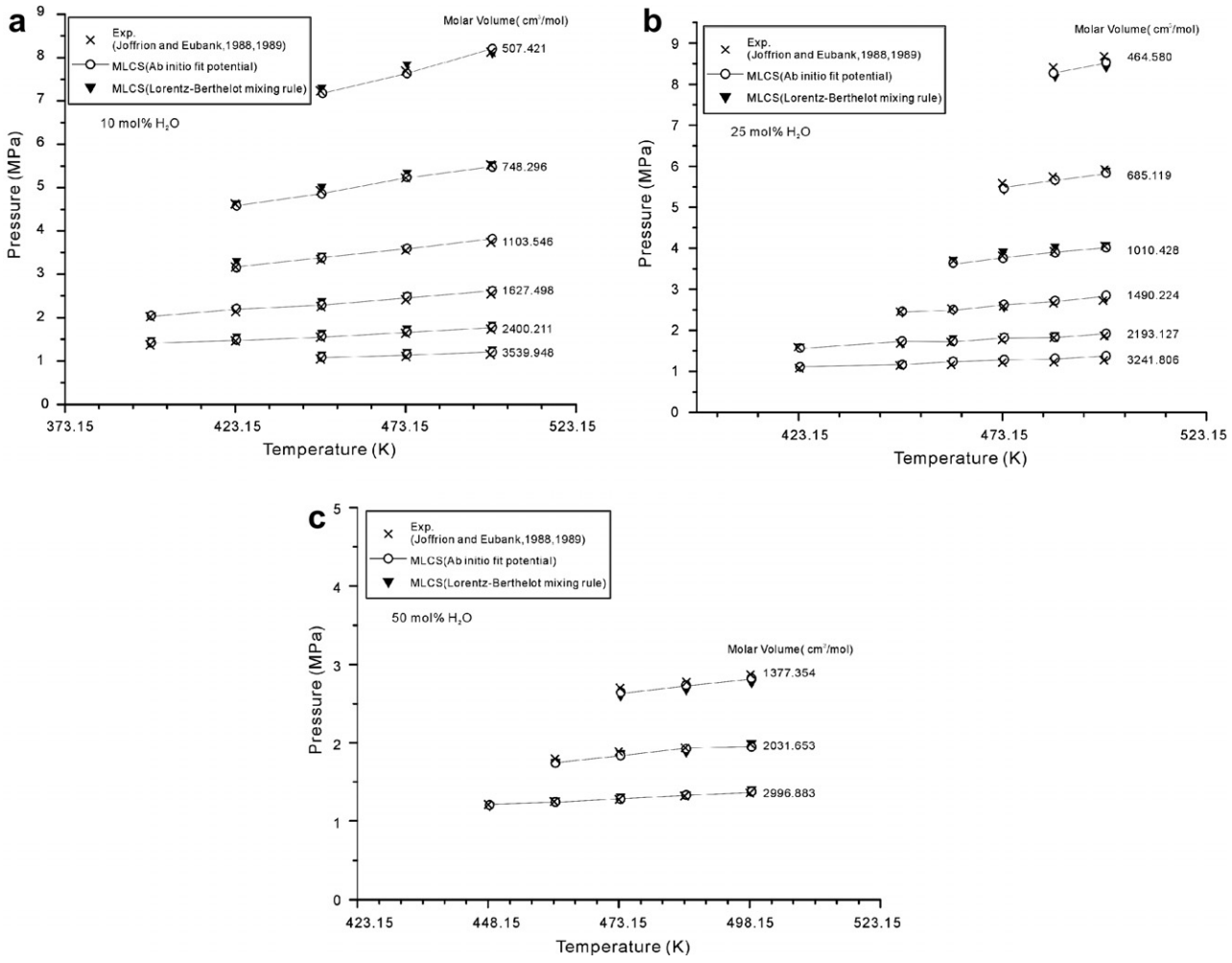

Fig. 7. Comparison of MLCS simulated molar volumes with the experimental data of Joffrion and Eubank (1988, 1989) for CH_4–H_2O fluids containing 10 (a), 25 (b), and 50 (c) mol% H_2O.

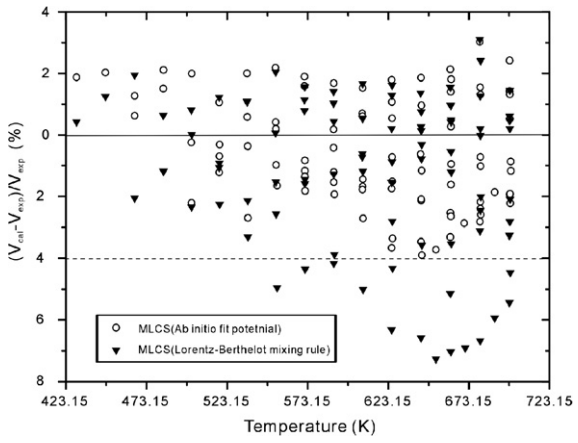

Fig. 8. Relative deviations of the simulated molar volumes from those measured by Fenghour et al. (1996).

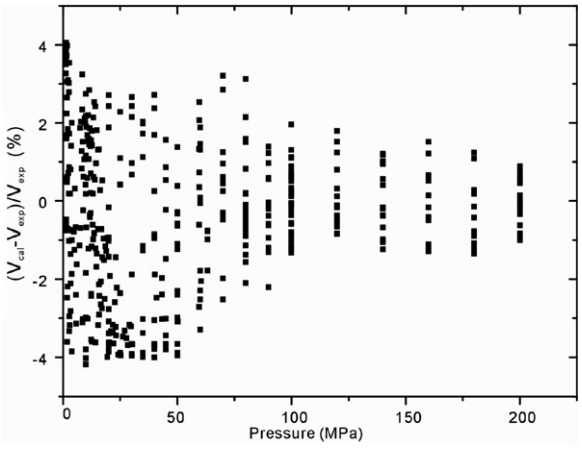

Fig. 9. Comparison of the simulated molar volumes with all experimental results.

(2005) are also plotted for comparison; our simulated isochors are quit close to her iso–Th lines and the deviation may be resulted from the volume discrepancy at the homogenization curve (Fig. 10).

6. EQUATION OF STATE

Equation of state (EOS) is a useful tool to study the geochemistry processes. A number of EOS's have been proposal for CH_4–H_2O system (Duan et al., 1992b; Grevel and Chatterjee, 1992). All of these EOS's were empirically fitted to the experimental data under 723 K and below 200 MPa and were restricted in the supercritical area. Duan et al. (1996) propose an EOS derived from theory for the pressures well above 1 GPa, but the maximum deviation of this EOS reaches 9.23% in density at $T = 1773.15$ K, $P = 10.0$ GPa and $x_{CH_4} = 0.2$.

In order to integrate latest experimental and our simulation data, we develop an EOS covering 673–2573 K and 0.01–10 GPa with or close to experimental accuracy. The general form is taken from Duan et al. (1992a,b) as

$$Z = \frac{PV}{RT} = 1 + \frac{BV_c}{V} + \frac{CV_c^2}{V^2} + \frac{DV_c^4}{V^4} + \frac{EV_c^5}{V^5} + \frac{FV_c^2}{V^2}\left(\beta + \frac{\gamma V_c^2}{V^2}\right)\exp\left(-\frac{\gamma V_c^2}{V^2}\right) \quad (15)$$

where R is the universal gas constant. For the end-members, the parameters (B, C, D,...) in Eq. (15) are calculated with the following equations:

$$B = a_1 + \frac{a_2}{T_r^2} + \frac{a_3}{T_r^3} \quad (16)$$

$$C = a_4 + \frac{a_5}{T_r^2} + \frac{a_6}{T_r^3} \quad (17)$$

$$D = a_7 + \frac{a_8}{T_r^2} + \frac{a_9}{T_r^3} \quad (18)$$

$$E = a_{10} + \frac{a_{11}}{T_r^2} + \frac{a_{12}}{T_r^3} \quad (19)$$

$$F = \frac{\alpha}{T_r^3} \quad (20)$$

$$T_r = \frac{T}{T_c} \quad (21)$$

$$V_c = \frac{RT_c}{P_c} \quad (22)$$

where T_c and P_c are the critical temperature and critical pressure, respectively. For water, $T_c = 647.25$ K, $P_c = 22.119$ MPa (Wagner and Prub, 2002). While for methane, $T_c = 190.551$ K, $P_c = 4.5992$ MPa (Friend et al., 1989).

Fifteen parameters in Eqs. (15)–(22) for each end-member, which are obtained from fitting to over 1500 available experimental and the simulation data points, are listed in Table 9. Consisted with the former EOS proposed by Duan and Zhang (2006) in CO_2–H_2O system, the parameters are divided into two TP regions with the boundary of 0.2 GPa to optimized the performance.

The mixing rule proposed by Duan et al. (1992b) are used to obtain the mixture parameters. Three empirical mixing parameters ($k_{1,ij}$, $k_{2,ijk}$ and $k_{3,ijk}$) are included to improve the accuracies and their relationships with temperature are listed in Table 10. The average deviation to simulation and experimental data is 0.83% and the maximum is 4%.

The partial fugacity coefficient ϕ_i at (T, P, x_i, V) can be derived with the following formula with developed EOS

$$\begin{aligned}\ln\phi_i - \ln\phi_i^{ref} = &-\ln Z + \ln Z^{ref} + \frac{(BV_c)'}{V}\Big|_{V^{ref}}^{V} + \frac{(CV_c^2)'}{2V^2}\Big|_{V^{ref}}^{V} + \frac{(DV_c^4)'}{4V^4}\Big|_{V^{ref}}^{V} \\ &+ \frac{(EV_c^5)'}{5V^5}\Big|_{V^{ref}}^{V} - \frac{1}{2\gamma V_c^2}\times\left((FV_c^2)'\beta + (FV_c^2)\beta'\right) \\ &\times\exp\left(-\frac{\gamma V_c^2}{V^2}\right)\Big|_{V^{ref}}^{V} - \frac{1}{2(\gamma V_c^2)^2}\times\left((FV_c^2)'(\gamma V_c^2)\right. \\ &\left.+(FV_c^2)(\gamma V_c^2)'\right)\times\left(\frac{\gamma V_c^2}{V^2}+1\right)\times\exp\left(-\frac{\gamma V_c^2}{V^2}\right)\Big|_{V^{ref}}^{V} \\ &- \frac{1}{2(\gamma V_c^2)^2}\times FV_c^2\times\beta\times\left(\gamma V_c^2 - (\gamma V_c^2)'\right)\times\left(\frac{\gamma V_c^2}{V^2}+1\right) \\ &\times\exp\left(-\frac{\gamma V_c^2}{V^2}\right)\Big|_{V^{ref}}^{V} - \frac{1}{2(\gamma V_c^2)^2}\times FV_c^2\times\left(\gamma V_c^2 - (\gamma V_c^2)'\right) \\ &\times\left(\frac{(\gamma V_c^2)^2}{V^4} + \frac{2\gamma V_c^2}{V^2} + 2\right)\times\exp\left(-\frac{\gamma V_c^2}{V^2}\right)\Big|_{V^{ref}}^{V}\end{aligned} \quad (23)$$

where $Z^{ref} = P^{ref}V^{ref}/RT$ is the compressibility factor at (T, P^{ref}, V^{ref}). The derivatives $((BV_c)', (CV_c)', \ldots)$ are listed in Table 11.

7. CONCLUSION

In this study, we adopted the molecular level computer simulation (MLCS) method to study the thermodynamic properties of the CH_4–H_2O system up to 2573 K and 10 GPa. More than two thousand of simulations were carried out and the results were used to compare with 1941 experimental points for CH_4 and 519 points for CH_4–H_2O mixtures in order to find the reliability of the MLCS method. The average deviation between simulated and experimental values is 0.83% for the binary $PVTx$ properties, which is equivalent to experimental uncertainty. After we confirmed the MLCS method in the study of the $PVTx$ properties of the CH_4–H_2O system and found the stable predictability of the simulation in wide TP range, we adopt this method to systematically study the $PVTx$ properties of the CH_4–H_2O binary system from 673 K and 0.05 GPa to 2573 K and 10 GPa. These data can serve as an important supplement to the experimental database.

Based on both the simulated and experimental data, we developed an equation of state for the CH_4–H_2O system, valid from 673 to 2573 K and from 0.001 to 10.0 GPa, with maximum errors less than 4% in density, and average errors less than 1% in density. The EOS covers a wide range of temperature and pressure and it is useful for deriving activities, the $PVTx$ properties, enthalpy and chemical potentials of this binary system up to very high temperatures and pressures. The interested readers can do online calculations or download the program of this EOS from the website: www.geochem-model.org/programs.htm.

Table 8
Molecular simulation results of the CH_4–H_2O system

Pressure (MPa)	673 K	698 K	723 K	773 K	873 K	973 K	1073 K	1173 K	1273 K	1373 K	1473 K
Molar volume of 20% CH_4 + 80% H_2O (cm^3/mol)											
50		76.02(1.33)		102.78(1.98)							
80		49.58(.91)		61.23(1.14)	79.37(1.81)	95.54(1.01)					
100		42.99(.61)		51.34(.89)	64.17(.87)	76.62(1.34)	89.05(1.40)	100.98(1.79)			
200		31.47(.36)		34.71(.22)	40.19(.40)	45.94(.46)	51.27(.44)	56.66(.76)	62.25(.59)	67.38(.58)	72.62(.94)
300	26.81(.18)	27.55(.16)	28.05(.16)	29.61(.17)	33.03(.36)	36.31(.27)	40.03(.37)	43.53(.55)	47.03(.47)	49.45(.52)	52.53(.50)
500	23.37(.08)	23.78(.12)	24.25(.09)	25.13(.16)	27.05(.12)	29.02(.17)	30.97(.20)	33.14(.17)	35.06(.16)	37.22(.17)	38.88(.20)
800	20.79(.05)	21.12(.07)	21.35(.04)	21.99(.07)	23.19(.10)	24.45(.11)	25.71(.10)	26.97(.11)	28.31(.13)	29.62(.13)	30.88(.22)
1000	19.74(.06)	19.97(.06)	20.26(.04)	20.71(.04)	21.74(.06)	22.75(.06)	23.75(.11)	24.82(.06)	25.83(.08)	26.89(.13)	27.87(.08)
2000	16.92(.02)	17.07(.02)	17.20(.04)	17.51(.03)	18.04(.05)	18.63(.05)	19.18(.04)	19.75(.05)	20.27(.03)	20.82(.07)	21.37(.04)
3000	15.51(.02)	15.61(.02)	15.73(.02)	15.94(.02)	16.34(.02)	16.74(.02)	17.16(.04)	17.56(.03)	17.95(.03)	18.30(.03)	18.73(.04)
4000			14.77(.02)	14.95(.02)	15.27(.01)	15.60(.02)	15.92(.02)	16.22(.03)	16.53(.02)	16.83(.01)	17.13(.03)
5000					14.51(.02)	14.78(.02)	15.07(.01)	15.31(.01)	15.57(.02)	15.82(.02)	16.06(.02)
6000								14.62(.01)	14.83(.01)	15.07(.02)	15.28(.02)
7000										14.46(.01)	14.66(.02)

Pressure (MPa)	1573 K	1673 K	1773 K	1873 K	1973 K	2073 K	2173 K	2273 K	2373 K	2473 K	2573 K
Molar volume of 20% CH_4 + 80% H_2O (cm^3/mol)											
200	77.92(.86)										
300	56.21(.59)	58.92(.93)	62.12(.54)	67.71(.99)							
500	40.07(.33)	41.44(.47)	43.31(.47)	47.33(.35)	49.38(.27)	51.14(.41)	53.24(.50)	55.08(.61)			
800	32.14(.22)	33.07(.19)	34.21(.17)	35.75(.23)	37.19(.19)	38.16(.17)	39.32(.15)	40.62(.36)	41.75(.38)	42.82(.31)	43.96(.46)
1000	28.99(.18)	29.89(.15)	30.95(.16)	31.91(.18)	32.86(.22)	33.92(.15)	34.83(.21)	35.82(.29)	36.77(.22)	37.70(.32)	38.45(.36)
2000	21.88(.04)	22.42(.05)	22.91(.09)	23.49(.12)	23.99(.06)	24.52(.09)	25.01(.14)	25.46(.11)	25.93(.13)	26.43(.07)	26.98(.11)
3000	19.09(.04)	19.45(.04)	19.79(.05)	20.20(.03)	20.49(.06)	20.89(.05)	21.25(.06)	21.58(.04)	21.90(.05)	22.29(.08)	22.64(.07)
4000	17.43(.03)	17.74(.02)	18.00(.03)	18.30(.04)	18.59(.03)	18.86(.05)	19.11(.07)	19.37(.03)	19.66(.06)	19.92(.06)	20.17(.05)
5000	16.32(.03)	16.56(.02)	16.80(.02)	17.03(.03)	17.27(.04)	17.49(.02)	17.73(.03)	17.95(.03)	18.16(.04)	18.39(.06)	18.60(.04)
6000	15.50(.01)	15.70(.02)	15.89(.02)	16.12(.03)	16.31(.02)	16.50(.02)	16.71(.02)	16.90(.02)	17.10(.03)	17.27(.05)	17.46(.04)
7000	14.84(.01)	15.03(.02)	15.21(.02)	15.38(.02)	15.57(.02)	15.75(.02)	15.91(.04)	16.09(.02)	16.26(.02)	16.41(.02)	16.58(.03)
8000	14.32(.02)	14.49(.02)	14.63(.01)	14.81(.02)	14.97(.02)	15.13(.03)	15.28(.02)	15.43(.02)	15.59(.02)	15.74(.03)	15.88(.02)
9000			14.17(.02)	14.32(.01)	14.47(.01)	14.62(.01)	14.75(.02)	14.90(.03)	15.03(.02)	15.17(.03)	15.30(.02)
10000					14.04(.02)	14.17(.01)	14.30(.01)	14.44(.02)	14.56(.01)	14.68(.01)	14.81(.02)

Pressure (MPa)	673 K	698 K	723 K	773 K	873 K	973 K	1073 K	1173 K	1273 K	1373 K	1473 K
Molar volume of 40% CH_4 + 60% H_2O (cm^3/mol)											
50		99.76(1.50)		118.36(2.09)							
80		66.64(.98)		79.19(1.58)	93.75(1.34)	108.82(2.05)					
100		57.87(.89)		66.58(1.26)	77.46(1.28)	89.74(1.53)	99.86(1.31)	107.94(1.48)			
200		39.52(.29)		43.15(.49)	48.44(.47)	53.83(.48)	59.19(.54)	64.76(.43)	69.88(.83)	75.12(.66)	79.20(1.25)
300	32.65(.14)	33.47(.18)	34.22(.16)	35.86(.18)	39.25(.15)	42.70(.36)	44.27(.39)	48.42(.45)	51.77(.45)	54.34(.50)	57.87(.41)
500	27.79(.06)	28.21(.15)	28.68(.09)	29.69(.12)	31.72(.11)	33.67(.13)	35.25(.28)	37.42(.28)	39.21(.19)	40.63(.34)	42.62(.24)
800	24.35(.08)	24.65(.06)	24.95(.09)	25.63(.07)	26.86(.09)	28.15(.11)	29.44(.11)	30.70(.14)	31.96(.16)	33.32(.19)	34.45(.21)
1000	22.97(.07)	23.22(.05)	23.48(.09)	23.98(.04)	25.07(.06)	26.11(.08)	27.13(.07)	28.20(.14)	29.17(.13)	30.14(.10)	31.28(.16)
2000	19.39(.02)	19.52(.04)	19.69(.04)	19.97(.03)	20.59(.04)	21.14(.04)	21.70(.05)	22.28(.06)	22.85(.08)	23.36(.06)	23.92(.06)

(*continued on next page*)

Table 8 (*continued*)

Pressure (MPa)	673 K	698 K	723 K	773 K	873 K	973 K	1073 K	1173 K	1273 K	1373 K	1473 K
3000	17.65(.03)	17.76(.02)	17.88(.03)	18.07(.03)	18.53(.02)	18.92(.02)	19.35(.04)	19.74(.04)	20.14(.03)	20.52(.03)	20.90(.04)
4000			16.73(.03)	16.89(.03)	17.26(.01)	17.58(.02)	17.91(.02)	18.24(.03)	18.55(.03)	18.84(.02)	19.13(.03)
5000					16.37(.03)	16.94(.01)	16.90(.02)	17.18(.02)	17.44(.02)	17.71(.02)	17.93(.02)
6000								16.38(.02)	16.60(.02)	16.82(.02)	17.05(.02)
7000										16.15(.03)	16.34(.01)

Pressure (MPa)	1573 K	1673 K	1773 K	1873 K	1973 K	2073 K	2173 K	2273 K	2373 K	2473 K	2573 K
Molar volume of 40% CH_4 + 60% H_2O (cm^3/mol)											
200	84.25(.71)										
300	60.94(.36)	63.18(.75)	66.42(.98)	71.75(.76)							
500	44.58(.29)	45.46(.34)	48.20(.33)	51.52(.33)	53.10(.58)	55.08(.35)	56.88(.78)	58.34(.60)			
800	35.36(.14)	36.41(.16)	37.55(.25)	39.33(.26)	40.38(.22)	41.49(.36)	42.90(.33)	43.69(.41)	44.89(.36)	45.96(.29)	47.11(.31)
1000	32.10(.19)	33.16(.13)	33.53(.13)	35.06(.15)	36.06(.25)	36.96(.18)	37.74(.21)	38.82(.15)	39.86(.31)	40.62(.23)	41.35(.23)
2000	24.41(.07)	24.94(.07)	25.44(.06)	25.93(.08)	26.52(.07)	26.93(.10)	27.39(.09)	27.94(.11)	28.37(.17)	28.85(.15)	29.33(.16)
3000	21.28(.04)	21.65(.04)	22.02(.03)	22.35(.07)	22.75(.06)	23.05(.05)	23.39(.06)	23.72(.09)	24.09(.09)	24.38(.09)	24.74(.08)
4000	19.45(.05)	19.73(.04)	20.01(.04)	20.30(.05)	20.57(.06)	20.81(.04)	21.12(.07)	21.39(.05)	21.62(.04)	21.89(.07)	22.15(.05)
5000	18.19(.03)	18.42(.04)	18.65(.04)	18.91(.04)	19.13(.04)	19.35(.04)	19.59(.04)	19.81(.04)	20.04(.05)	20.24(.05)	20.44(.04)
6000	17.26(.03)	17.48(.02)	17.70(.03)	17.88(.03)	18.08(.03)	18.27(.03)	18.45(.04)	18.66(.02)	18.83(.03)	19.01(.04)	19.21(.04)
7000	16.53(.02)	16.73(.02)	16.91(.03)	17.08(.03)	17.26(.02)	17.44(.03)	17.60(.02)	17.77(.02)	17.93(.04)	18.11(.02)	18.24(.02)
8000	15.96(.01)	16.10(.02)	16.27(.02)	16.43(.02)	16.59(.03)	16.75(.03)	16.90(.02)	17.05(.03)	17.22(.02)	17.37(.03)	17.49(.03)
9000			15.75(.02)	15.89(.02)	16.05(.03)	16.19(.02)	16.32(.01)	16.46(.02)	16.59(.03)	16.74(.03)	16.87(.02)
10000					15.58(.02)	15.71(.02)	15.83(.01)	15.96(.02)	16.09(.02)	16.21(.02)	16.33(.02)

Pressure (MPa)	673 K	698 K	723 K	773 K	873 K	973 K	1073 K	1173 K	1273 K	1373 K	1473 K
Molar volume of 60% CH_4 + 40% H_2O (cm^3/mol)											
50		119.59(2.10)		139.04(2.55)							
80		81.98(1.18)		91.50(.95)	104.60(1.97)	117.92(1.91)					
100		69.78(.56)		77.81(.80)	87.98(1.43)	98.53(1.57)	108.98(1.28)	118.12(1.09)			
200		46.91(.40)		50.78(.27)	55.74(.40)	60.65(.70)	65.87(.96)	70.63(.61)	74.67(1.12)	80.11(1.12)	84.83(1.22)
300	38.34(.28)	39.23(.28)	40.07(.18)	41.80(.27)	45.03(.39)	48.32(.24)	50.98(.37)	54.83(.41)	56.46(.43)	60.18(.76)	63.00(.65)
500	32.22(.14)	32.79(.11)	33.17(.12)	34.17(.19)	36.25(.18)	38.17(.26)	40.28(.23)	42.11(.26)	43.96(.38)	43.93(.37)	46.32(.26)
800	27.93(.07)	28.33(.09)	28.62(.08)	29.23(.07)	30.56(.08)	31.89(.13)	33.05(.14)	34.40(.16)	35.59(.16)	36.86(.16)	38.04(.15)
1000	26.29(.06)	26.57(.06)	26.85(.07)	27.33(.06)	28.49(.10)	29.45(.09)	30.48(.09)	31.49(.13)	32.47(.13)	33.55(.15)	34.45(.17)
2000	22.05(.03)	22.21(.03)	22.34(.05)	22.62(.04)	23.24(.03)	23.82(.03)	24.39(.04)	24.93(.07)	25.49(.04)	25.97(.06)	26.54(.07)
3000	20.01(.02)	20.11(.03)	20.24(.02)	20.46(.03)	20.89(.03)	21.32(.03)	21.68(.03)	22.12(.04)	22.51(.04)	22.89(.05)	23.26(.05)
4000			18.91(.02)	19.08(.03)	19.44(.02)	19.77(.03)	20.11(.02)	20.40(.03)	20.72(.03)	21.02(.02)	21.32(.03)
5000					18.41(.02)	18.70(.02)	18.97(.02)	19.23(.02)	19.49(.03)	19.74(.02)	20.00(.03)
6000								18.33(.02)	18.57(.02)	18.79(.02)	18.99(.02)
7000										18.04(.01)	18.23(.03)

Pressure (MPa)	1573 K	1673 K	1773 K	1873 K	1973 K	2073 K	2173 K	2273 K	2373 K	2473 K	2573 K
Molar volume of 60% CH_4 + 40% H_2O (cm^3/mol)											
200	88.62(.90)										
300	65.53(.90)	68.60(.77)	72.00(1.08)	76.10(.54)							

500	49.18(.28)	50.55(.45)	52.12(.25)	54.97(.43)	56.98(.50)	58.55(.70)	60.23(.52)	61.84(.43)			
800	39.19(.26)	40.31(.20)	41.21(.23)	42.47(.36)	43.97(.28)	44.99(.38)	46.05(.34)	46.91(.40)	48.07(.43)	49.43(.54)	50.36(.37)
1000	35.46(.29)	36.36(.16)	37.21(.22)	38.36(.25)	39.07(.22)	40.10(.33)	40.90(.23)	41.79(.25)	42.76(.26)	43.62(.41)	44.42(.21)
2000	27.05(.06)	27.54(.09)	28.10(.11)	28.58(.12)	29.09(.12)	29.56(.07)	30.03(.10)	30.50(.11)	31.05(.11)	31.49(.07)	31.93(.11)
3000	23.60(.03)	24.00(.06)	24.33(.03)	24.71(.04)	25.06(.08)	25.42(.07)	25.72(.04)	26.04(.09)	26.43(.08)	26.73(.11)	27.07(.07)
4000	21.60(.03)	21.91(.02)	22.17(.04)	22.48(.03)	22.70(.04)	22.95(.05)	23.27(.05)	23.56(.07)	23.81(.03)	24.03(.04)	24.33(.05)
5000	20.24(.04)	20.49(.02)	20.72(.03)	20.94(.04)	21.18(.02)	21.40(.04)	21.62(.05)	21.85(.05)	22.03(.03)	22.29(.06)	22.50(.07)
6000	19.21(.03)	19.41(.03)	19.62(.02)	19.84(.04)	20.03(.04)	20.21(.01)	20.41(.03)	20.60(.03)	20.80(.04)	20.97(.05)	21.13(.06)
7000	18.41(.03)	18.59(.03)	18.76(.02)	18.96(.03)	19.16(.03)	19.30(.02)	19.48(.02)	19.64(.03)	19.80(.03)	19.98(.02)	20.14(.05)
8000	17.76(.02)	17.93(.02)	18.10(.02)	18.24(.02)	18.42(.03)	18.57(.03)	18.73(.03)	18.87(.02)	19.01(.03)	19.17(.03)	19.34(.04)
9000			17.51(.02)	17.67(.03)	17.81(.02)	17.97(.02)	18.09(.02)	18.22(.03)	18.36(.02)	18.49(.02)	18.64(.03)
10000					17.29(.02)	17.42(0.5)	17.55(.02)	17.67(.02)	17.82(.03)	17.92(.03)	18.05(.02)

Pressure (MPa)	673 K	698 K	723 K	773 K	873 K	973 K	1073 K	1173 K	1273 K	1373 K	1473 K
Molar volume of 80% CH_4 + 20% H_2O (cm^3/mol)											
50		133.51(2.22)		146.94(2.31)							
80		91.27(.84)		101.09(1.35)	113.07(1.03)	125.51(1.53)					
100		79.06(.95)		86.43(.98)	95.51(1.18)	105.13(1.13)	113.99(1.23)	122.63(1.41)			
200		53.46(.21)		57.17(.38)	61.84(.49)	66.33(.45)	71.19(.62)	75.77(.55)	80.67(.88)	84.64(.54)	88.98(.97)
300	43.88(.33)	44.47(.19)	45.44(.25)	47.17(.27)	50.28(.21)	53.49(.46)	56.61(.37)	59.60(.33)	63.09(.41)	66.00(.45)	68.70(.38)
500	36.45(.16)	36.91(.10)	37.44(.13)	38.51(.12)	40.50(.23)	42.36(.25)	44.22(.20)	46.06(.16)	48.07(.26)	49.63(.29)	51.79(.34)
800	31.54(.08)	31.81(.08)	32.22(.09)	32.86(.07)	34.12(.08)	35.30(.18)	36.62(.16)	37.80(.17)	39.12(.13)	40.09(.20)	41.40(.19)
1000	29.54(.06)	29.84(.05)	30.14(.08)	30.68(.07)	31.73(.08)	32.77(.07)	33.82(.14)	34.80(.11)	35.83(.13)	36.71(.16)	37.70(.12)
2000	24.71(.02)	24.83(.04)	25.00(.04)	25.31(.03)	25.92(.05)	26.51(.04)	27.08(.03)	27.63(.06)	28.15(.04)	28.73(.06)	29.25(.05)
3000	22.41(.03)	22.52(.03)	22.63(.03)	22.87(.02)	23.29(.02)	23.72(.04)	24.14(.05)	24.53(.03)	24.92(.04)	25.32(.05)	25.67(.03)
4000			21.15(.02)	21.32(.02)	21.67(.02)	22.02(.02)	22.35(.02)	22.67(.02)	22.99(.04)	23.26(.02)	23.59(.05)
5000					20.53(.03)	20.83(.03)	21.09(.02)	21.36(.02)	21.63(.02)	21.89(.03)	22.13(.03)
6000								20.39(.02)	20.62(.02)	20.84(.02)	21.07(.03)
7000										20.01(.02)	20.21(.02)

Pressure (MPa)	1573 K	1673 K	1773 K	1873 K	1973 K	2073 K	2173 K	2273 K	2373 K	2473 K	2573 K
Molar volume of 80% CH_4 + 20% H_2O (cm^3/mol)											
200	93.66(.89)										
300	71.47(.50)	74.36(.63)	77.20(.55)	81.21(.54)							
500	53.54(.33)	55.05(.50)	56.84(.40)	59.07(.14)	60.15(.49)	62.16(.72)	63.90(.54)	65.40(.65)			
800	42.46(.25)	43.49(.18)	44.82(.24)	45.91(.32)	47.09(.30)	48.26(.38)	49.62(.28)	50.30(.42)	51.51(.37)	52.68(.32)	53.47(.44)
1000	38.68(.18)	39.34(.29)	40.58(.37)	41.34(.23)	42.28(.24)	43.22(.26)	43.98(.31)	45.04(.25)	45.82(.34)	46.75(.14)	47.62(.35)
2000	29.71(.08)	30.28(.08)	30.70(.09)	31.29(.09)	31.77(.14)	32.24(.12)	32.74(.08)	33.22(.11)	33.61(.14)	34.09(.07)	34.58(.15)
3000	26.02(.05)	26.40(.05)	26.76(.05)	27.11(.07)	27.48(.07)	27.79(.06)	28.21(.07)	28.45(.04)	28.82(.07)	29.16(.11)	29.53(.10)
4000	23.86(.04)	24.16(.05)	24.45(.05)	24.75(.05)	24.98(.06)	25.28(.04)	25.51(.08)	25.82(.06)	26.08(.06)	26.36(.06)	26.54(.09)
5000	22.37(.03)	22.62(.04)	22.88(.04)	23.10(.04)	23.33(.04)	23.57(.05)	23.76(.05)	24.00(.05)	24.27(.04)	24.43(.06)	24.63(.05)
6000	21.28(.03)	21.47(.03)	21.70(.04)	21.88(.03)	22.07(.04)	22.29(.03)	22.49(.03)	22.66(.04)	22.87(.03)	23.05(.04)	23.25(.03)
7000	20.40(.02)	20.59(.02)	20.76(.02)	20.96(.04)	21.11(.03)	21.30(.02)	21.48(.04)	21.67(.03)	21.82(.02)	21.99(.04)	22.15(.05)
8000	19.69(.02)	19.86(.02)	20.04(.02)	20.18(.03)	20.34(.03)	20.51(.02)	20.67(.03)	20.80(.03)	20.96(.03)	21.09(.03)	21.25(.03)
9000			19.40(.02)	19.55(.03)	19.71(.02)	19.83(.01)	19.97(.02)	20.11(.02)	20.26(.02)	20.41(.03)	20.54(.03)

10000					19.14(.02)	19.27(.01)	19.41(.02)	19.53(.02)	19.66(.01)	19.79(.02)	19.91(.03)

(*continued on next page*)

Table 8 (*continued*)

Pressure (MPa)	673 K	698 K	723 K	773 K	873 K	973 K	1073 K	1173 K	1273 K	1373 K	1473 K
Molar volume of pure CH_4 (cm^3/mol)											
50		138.13(1.19)		153.02(1.39)							
80		97.68(.79)		106.39(.50)	117.89(.54)	129.25(1.02)					
100		84.34(.45)		91.24(.51)	100.43(.71)	109.52(.57)	118.67(.64)	127.92(.71)			
200		57.93(.15)		61.41(.41)	66.13(.23)	70.78(.37)	75.33(.23)	79.52(.48)	84.30(.53)	88.50(.45)	92.86(.31)
300	47.99(.09)	48.82(.21)	49.63(.23)	51.19(.12)	54.30(.20)	57.48(.15)	60.39(.22)	63.39(.22)	66.28(.33)	69.22(.34)	72.29(.25)
500	40.20(.10)	40.65(.11)	41.14(.13)	42.15(.12)	44.06(.12)	45.95(.12)	47.76(.13)	49.69(.14)	51.46(.13)	53.29(.15)	55.04(.13)
800	34.83(.05)	35.15(.05)	35.46(.09)	36.10(.05)	37.38(.09)	38.60(.09)	39.86(.07)	41.01(.09)	42.20(.12)	43.41(.14)	44.60(.09)
1000	32.67(.04)	32.96(.03)	33.24(.05)	33.76(.06)	34.79(.09)	35.88(.07)	36.84(.07)	37.84(.09)	38.85(.10)	39.78(.07)	40.76(.13)
2000	27.32(.02)	27.47(.01)	27.63(.03)	27.95(.04)	28.54(.05)	29.13(.02)	29.69(.04)	30.27(.05)	30.80(.03)	31.34(.02)	31.87(.06)
3000	24.79(.02)	24.91(.02)	25.03(.03)	25.25(.03)	25.71(.03)	26.13(.02)	26.53(.02)	26.94(.02)	27.33(.02)	27.73(.04)	28.10(.03)
4000			23.40(.02)	23.57(.01)	23.93(.02)	24.27(.02)	24.61(.01)	24.92(.02)	25.24(.03)	25.56(.04)	25.84(.02)
5000					22.68(.01)	22.96(.02)	23.25(.02)	23.51(.02)	23.78(.02)	24.05(.02)	24.30(.02)
6000								22.47(.01)	22.69(.01)	22.93(.01)	23.15(.01)
7000										22.04(.02)	22.23(.01)

Pressure (MPa)	1573 K	1673 K	1773 K	1873 K	1973 K	2073 K	2173 K	2273 K	2373 K	2473 K	2573 K
Molar volume of pure CH_4 (cm^3/mol)											
200	97.20(.41)										
300	75.40(.35)	78.18(.26)	80.88(.46)	83.87(.28)							
500	56.92(.16)	58.59(.16)	60.40(.11)	62.17(.21)	63.95(.25)	65.79(.32)	67.44(.23)	69.13(.30)			
800	45.73(.14)	46.94(.17)	48.00(.12)	49.13(.13)	50.26(.13)	51.34(.12)	52.56(.19)	53.55(.14)	54.67(.11)	55.74(.24)	56.90(.17)
1000	41.69(.07)	42.67(.11)	43.55(.08)	44.57(.10)	45.41(.15)	46.24(.13)	47.18(.13)	48.14(.14)	49.05(.16)	49.88(.14)	50.75(.13)
2000	32.38(.03)	32.91(.04)	33.40(.05)	33.95(.05)	34.41(.02)	34.89(.06)	35.39(.09)	35.89(.05)	36.34(.07)	36.80(.07)	37.29(.08)
3000	28.47(.03)	28.86(.02)	29.21(.04)	29.57(.04)	29.94(.04)	30.27(.04)	30.62(.03)	30.95(.05)	31.33(.05)	31.64(.03)	31.97(.04)
4000	26.16(.03)	26.45(.02)	26.75(.02)	27.01(.03)	27.31(.03)	27.59(.03)	27.86(.02)	28.13(.03)	28.39(.03)	28.66(.02)	28.94(.03)
5000	24.56(.01)	24.81(.02)	25.05(.01)	25.30(.02)	25.53(.02)	25.75(.02)	26.00(.02)	26.23(.02)	26.44(.03)	26.66(.03)	26.89(.03)
6000	23.37(.01)	23.58(.01)	23.79(.01)	23.99(.02)	24.20(.01)	24.42(.02)	24.60(.01)	24.80(.02)	24.99(.02)	25.20(.02)	25.38(.03)
7000	22.43(.01)	22.62(.01)	22.80(.01)	22.99(.02)	23.18(.02)	23.35(.02)	23.53(.03)	23.71(.01)	23.89(.01)	24.05(.01)	24.23(.02)
8000	21.66(.01)	21.83(.01)	22.00(.02)	22.17(.01)	22.34(.02)	22.49(.02)	22.65(.01)	22.81(.01)	22.97(.02)	23.13(.01)	23.26(.01)

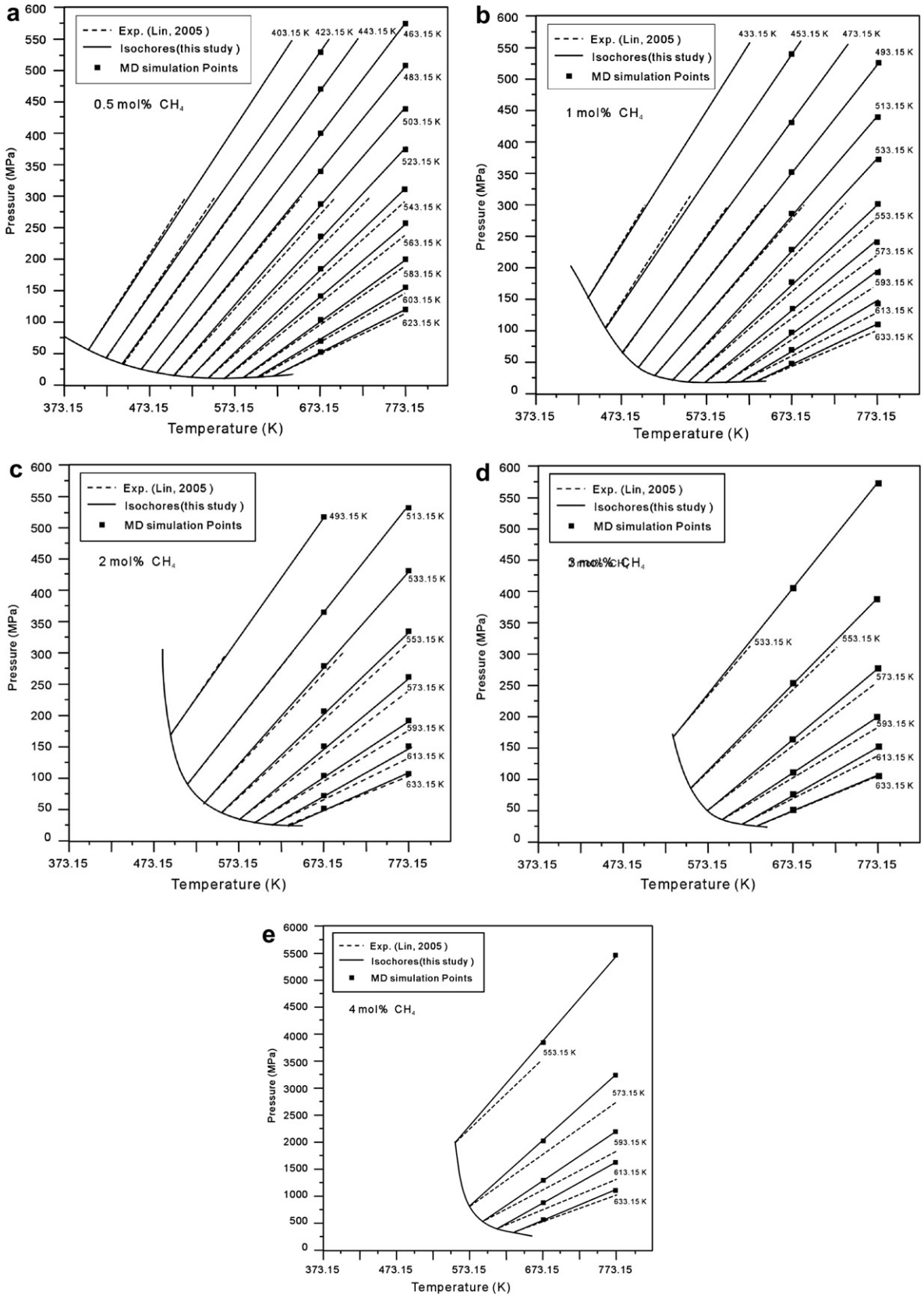

Fig. 10. Isochore for CH_4–H_2O fluid inclusions containing 0.5 (a), 1 (b), 2 (c), 3 (d), and 4 (e) mol% CH_4.

Table 9
Parameters of the new EOS in this study Eqs. (15)–(22)

Pressure range	Parameters	H_2O	CO_2
0–0.02 GPa	a_1	4.38269941E−02	8.86065479E−02
	a_2	−1.68244362E−01	−7.91394224E−01
	a_3	−2.36923373E−01	5.83516966E−01
	a_4	1.13027462E−02	1.56779057E−02
	a_5	−7.67764181E−02	−5.18627568E−02
	a_6	9.71820593E−02	3.09262718E−02
	a_7	6.62674916E−05	1.19654015E−04
	a_8	1.06637349E−03	1.74351225E−03
	a_9	−1.23265258E−03	−1.16629734E−03
	a_{10}	−8.93953948E−06	−3.91950486E−06
	a_{11}	−3.88124606E−05	1.21774330E−04
	a_{12}	5.61510206E−05	−1.98683200E−04
	a_{13}	7.51274488E−03	3.28944589E−02
	a_{14}	2.51598931E+00	−9.15565822E+00
	γ	3.94000000E−02	5.08910000E−01
0.2–10.0 GPa	a_1	4.68071541E−02	9.21611054E−02
	a_2	−2.81275941E−01	2.34583366E−01
	a_3	−2.43926365E−01	−1.65704237E+00
	a_4	1.10016958E−02	1.40183938E−02
	a_5	−3.86603525E−02	−2.57788936E−01
	a_6	9.30095461E−02	5.15782153E+00
	a_7	−1.15747171E−05	1.20922301E−04
	a_8	4.19873848E−04	3.18404732E−03
	a_9	−5.82739501E−04	−4.10314927E−02
	a_{10}	1.00936000E−06	−4.66789559E−06
	a_{11}	−1.01713593E−05	2.22799193E−04
	a_{12}	1.63934213E−05	6.12540167E−04
	a_{13}	−4.49505919E−02	−3.01741577E+00
	a_{14}	−3.15028174E−01	1.48878165E+00
	γ	1.25000000E−02	1.51800000E−02

Table 10
The binary interaction parameters of the CH_4–H_2O system when $673 \leqslant T \leqslant 2573$ K

Pressure range	Parameters
0–0.2 GPa	$k_1 = -1.5763\text{E+}03 - 1.6440\text{E+}00\ T + -5.2138\text{E−}04\ T^2 - 4.7800\text{E+}05/T$
	$k_2 = -6.4177\text{E+}01 + 6.9174\text{E−}02\ T - 2.2865\text{E−}05\ T^2 + 1.9492\text{E+}04/T$
	$k_3 = 2.3125\text{E+}00 + -1.2184\text{E−}03\ T - 5.5849\text{E−}08\ T^2 - 5.5940\text{E+}02\ /T$
0.2–10.0 GPa	$k_1 = 3.6644\text{E+}01 - 2.6743\text{E−}02\ T + 6.0670\text{E−}06\ T^2 - 1.1661\text{E+}04/T$
	$k_2 = -2.7076\text{E+}00 + 3.2349\text{E−}03\ T - 8.9888\text{E−}07\ T^2 + 1.1557\text{E+}03/T$
	$k_3 = 1.0$

Table 11
The mixing rule for the EOS of the CH_4–H_2O mixture and derivatives in Eq. (15)

$BV_c = \sum_i \sum_j x_i x_j B_{ij} V_{cij}$	$B_{ij} = [(B_i^{1/3} + B_j^{1/3})/2]^3 k_{1,ij}$
$(BV_c)' = 2\sum_j x_j B_{ij} V_{cij}$	$k_{1,ij} = 1.0 \quad (i = j)$
	$V_{cij} = [(V_{ci}^{1/3} + V_{cj}^{1/3})/2]^3$
$CV_c^2 = \sum_i \sum_j \sum_k x_i x_j x_k C_{ijk} V_{cijk}^2$	$C_{ijk} = [(C_i^{1/3} + C_j^{1/3} + C_k^{1/3})/3]^3 k_{2,ijk}$
$(CV_c^2)' = 3\sum_j \sum_k x_j x_k C_{ijk} V_{cijk}^2$	$k_{2,ijk} = 1.0 \quad (i = j = k)$
	$k_{2,iij} = k_{2,jji}$
	$V_{cijk} = [(V_{ci}^{1/3} + V_{cj}^{1/3} + V_{ck}^{1/3})/3]^3$
$DV_c^4 = \sum_i \sum_j \sum_k \sum_l \sum_m x_i x_j x_k x_l x_m D_{ijklm} V_{cijklm}^4$	$D_{ijklm} = [(D_i^{1/3} + D_j^{1/3} + D_k^{1/3} + D_l^{1/3} + D_m^{1/3})/5]^3$
$(DV_c^4)' = 5\sum_j \sum_k \sum_l \sum_m x_j x_k x_l x_m D_{ijklm} V_{cijklm}^4$	$V_{cijk} = [(V_{ci}^{1/3} + V_{cj}^{1/3} + V_{ck}^{1/3} + V_{cl}^{1/3} + V_{cm}^{1/3})/5]^3$
$EV_c^5 = \sum_i \sum_j \sum_k \sum_l \sum_m \sum_n x_i x_j x_k x_l x_m x_n E_{ijklmn} V_{cijklmn}^5$	$E_{ijklm} = [(E_i^{1/3} + E_j^{1/3} + E_k^{1/3} + E_l^{1/3} + E_m^{1/3} + E_n^{1/3})/6]^3$
$(EV_c^5)' = 6\sum_j \sum_k \sum_l \sum_m \sum_n x_j x_k x_l x_m x_n E_{ijklmn} V_{cijklmn}^5$	$V_{cijk} = [(V_{ci}^{1/3} + V_{cj}^{1/3} + V_{ck}^{1/3} + V_{cl}^{1/3} + V_{cm}^{1/3} + V_{cn}^{1/3})/6]^3$
$FV_c^2 = \sum_i \sum_j x_i x_j F_{ij} V_{cij}^2$	$F_{ijk} = [(F_i^{1/3} + F_j^{1/3})/2]^3$
$(FV_c^2)' = 2\sum_j x_j F_{ij} V_{cij}^2$	$V_{cij} = [(V_{ci}^{1/3} + V_{cj}^{1/3})/2]^3$
$\beta = \sum_i x_i \beta_i$	
$\beta' = \beta_i$	
$\gamma V_c^2 = \sum_i \sum_j \sum_k x_i x_j x_k \gamma_{ijk} V_{cijk}^2$	$\gamma_{ijk} = [(\gamma_i^{1/3} + \gamma_j^{1/3} + \gamma_k^{1/3})/3]^3 k_{3,ijk}$
$(\gamma V_c^2)' = 3\sum_j \sum_k x_j x_k \gamma_{ijk} V_{cijk}^2$	$k_{3,ijk} = 1.0 \quad (i = j = k)$
	$k_{3,iij} = k_{3,jji}$
	$V_{cijk} = [(V_{ci}^{1/3} + V_{cj}^{1/3} + V_{ck}^{1/3})/3]^3$

ACKNOWLEDGMENTS

We thank Drs. I-Ming Chou, James Rustad and two anonymous reviewers for their constructive suggestions for improving the paper. This work is supported by Zhenhao Duan's "Outstanding Young Scientist Funds" (No. 40225008) and "Key Project Funds" (No. 40537032) awarded by National Science Foundation of China. We acknowledge the generous help of Dr. Bernhardt L. Trout for providing ab initio data of the CH_4–H_2O complex.

REFERENCES

Abdulagatov I. M., Bazaev A. R., Gasanov R. K., and Ramazanova A. E. (1996) Measurements of the (p,ρ,T) properties and virial coefficients of pure water, methane, *n*-hexane, *n*-octane, benzene, and of their aqueous mixtures in the supercritical region. *J. Chem. Thermodyn.* **28**(9), 1037–1057.

Abdulagatov I. M., Bazaev A. R., and Ramazanova A. E. (1993a) *P–V–T–X* measurements of aqueous mixtures at supercritical conditions. *Int. J. Thermophys.* **14**(2), 231–250.

Abdulagatov I. M., Bazaev A. R., and Ramazanova A. E. (1993b) Volumetric properties and virial coefficients of (water + methane). *J. Chem. Thermodyn.* **25**(2), 249–259.

Achtermann H. J., Bose T. K., Rogener H., and Starnaud J. M. (1986) Precise determination of the compressibility factor of methane, nitrogen, and their mixtures from refractive-index measurements. *Int. J. Thermophys.* **7**(3), 709–720.

Andersen H. C. (1983) Rattle: a "Velocity" version of the Shake algorithm for molecular dynamics calculations. *J. Comput. Phys.* **52**, 24–34.

Angus S., Armstrong B., and Reuck K. M. (1978) International thermodynamic tables of fluid state—5 methane. *Int. Union Pure Appl. Chem. Chem. Data Series*, 16.

Belonoshko A., and Saxena S. K. (1991) A molecular-dynamics study of the pressure–volume–temperature properties of supercritical fluids.2. CO_2, CH_4, CO, O_2, and H_2. *Geochim. Cosmochim. Acta* **55**(11), 3191–3208.

Birkett G. R., and Do D. D. (2004) PVT behaviour of fluids with potential models optimised for phase equilibria. *Fluid Phase Equilibr.* **224**(2), 199–212.

Boulougouris G. C., Economou I. G., and Theodorou D. N. (1998) Engineering a molecular model for water phase equilibrium over a wide temperature range. *J. Phys. Chem. B* **102**(6), 1029–1035.

Cao Z. T., Tester J. W., and Trout B. L. (2001) Computation of the methane-water potential energy hypersurface via ab initio methods. *J. Chem. Phys.* **115**(6), 2550–2559.

Carroll M. R., and Holloway, J. R. (1994) Volatiles in Magmas. In *Rev. Mineral.* (ed. P. H. Ribbe). Mineralogical Society of America.

Chen B., Martin M. G., and Siepmann J. I. (1998) Thermodynamic properties of the Williams, OPLS-AA, and MMFF94 all-atom force fields for normal alkanes. *J. Phys. Chem. B* **102**(14), 2578–2586.

Christotoforakos, M. (1985). Uberkritische systeme uder hohem Drucj. Eine statistisch-thermodynamisch entwickelte Zustandsgleichung und experimentelle Untersuchungen. Ph.D University of Karlsruhe.

Ciccotti G., Martyna G. J., Melchionna S., and Tuckerman M. E. (2001) Constrained isothermal–isobaric molecular dynamics with full atomic virial. *J. Phys. Chem. B* **105**(28), 6710–6715.

Deffet L., Liangne L., and Ficks F. (1964) La compressibilite du methane jusqu'a 3000 kg/cm^2. *Ind. Chim. Belg.-Belgische Chem. Ind.* **9**, 879–888.

Dore L., Cohen R. C., Schmuttenmaer C. A., Busarow K. L., Elrod M. J., Loeser J. G., and Saykally R. J. (1994) Far-infrared vibration–rotation-tunneling spectroscopy and internal dynamics of methane–water—a prototypical hydrophobic system. *J. Chem. Phys.* **100**(2), 863–876.

Douslin D. R., Harrison R. H., Moore R. T., and MuCullough J. (1964) *P–V–T* relations for methane. *J. Chem. Eng. Data* **9**(3), 358–363.

Duan Z. H., Moller N., and Weare J. H. (1992a) An equation of state for the CH_4–CO_2–H_2O system: I. Pure systems from 0 to 1000 °C and 0 to 8000 bar. *Geochim. Cosmochim. Acta* **56**(7), 2605–2617.

Duan Z. H., Moller N., and Weare J. H. (1992b) An equation of state for the CH_4–CO_2–H_2O system: II. Mixtures from 50 to 1000 °C and 0 to 1000 bar. *Geochim. Cosmochim. Acta* **56**(7), 2619–2631.

Duan Z. H., Moller N., and Weare J. H. (1996) A general equation of state for supercritical fluids and molecular dynamics simulation of mixture PVTX properties. *Geochim. Cosmochim. Acta* **60**(7), 1209–1216.

Duan Z. H., and Zhang Z. G. (2006) Equation of state of the H_2O, CO_2, and H_2O–CO_2 systems up to 10 GPa and 2573.15 K: molecular dynamics simulations with ab initio potential surface. *Geochim. Cosmochim. Acta* **70**(9), 2311–2324.

Dubessy J., Buschaert S., Lamb W., Pironon J., and Thiery R. (2001) Methane-bearing aqueous fluid inclusions: Raman analysis, thermodynamic modelling and application to petroleum basins. *Chem. Geol.* **173**(1–3), 193–205.

Errington J. R., Boulougouris G. C., Economou I. G., Panagiotopoulos A. Z., and Theodorou D. N. (1998) Molecular simulation of phase equilibria for water–methane and water–ethane mixtures. *J. Phys. Chem. B* **102**(44), 8865–8873.

Fenghour A., Wakeham W. A., and Watson J. T. R. (1996) Densities of (water plus methane) in the temperature range 430 K to 699 K and at pressures up to 30 MPa. *J. Chem. Thermodyn.* **28**(4), 447–458.

Fitzwater S., and Bartell L. S. (1976) Representations of molecular force fields. II.A modified Urey–Bradley field and an examination of Allinger's gauche hydrogen hypothesis. *J. Am. Chem. Soc.* **98**(17), 5107–5115.

Friend D. G., Ely J. F., and lngham H. (1989) Thermophysical properties of methane. *J. Phys. Chem. Ref. Data* **18**(2), 583–638.

Grevel K. D. (1993) Modified Redlich–Kwong equations of state for CH_4 and CH_4–H_2O fluid mixtures. *Neues Jahrb. Mineral. Monat.* **10**, 462–480.

Grevel K. D., and Chatterjee N. D. (1992) A modified Redlich–Kwong equation of state for H_2–H_2O fluid mixtures at high-pressures and at temperatures above 400 °C. *Eur. J. Mineral.* **4**(6), 1303–1310.

Hedenquist J. W., and Lowenstern J. B. (1994) The role of magmas in the formation of hydrothermal ore deposits. *Nature* **370**, 519–526.

Hnedkovsky L., Wood R. H., and Majer V. (1996) Volumes of aqueous solutions of CH_4, CO_2, H_2S, and NH_3 at temperatures from 298.15 K to 705 K and pressures to 35 MPa. *J. Chem. Thermodyn.* **28**(2), 125–142.

Joffrion L. L., and Eubank P. T. (1988) *P–V–T* data and virial-coefficients for gaseous methane-water mixtures with correction for adsorption effects. *Fluid Phase Equilibr.* **43**(2-3), 263–294.

Joffrion L. L., and Eubank P. T. (1989) Compressibility factors, densities, and residual thermodynamic properties for methane water mixtures. *J. Chem. Eng. Data* **34**(2), 215–220.

Jorgensen W. L., Madura J. D., and Swenson C. J. (1984) Optimized intermolecular potential functions for liquid hydrocarbons. *J. Am. Chem. Soc.* **106**(22), 6638–6646.

Kaminski G., Duffy E. M., Matsui T., and Jorgensen W. L. (1994) Free-energies of hydration and pure liquid properties of hydrocarbons from the OPLS all-atom model. *J. Phys. Chem.* **98**(49), 13077–13082.

Kelley D. S. (1996) Methane-bearing fluids in the oceanic crust: Gabbro-hosted fluid inclusions from the southwest Indian Ridge. *J. Geophys. Res.* **101**, 2943–2962.

Kisch H. J., and Van Den Kerkhof A. M. (1991) CH_4-rich inclusions from quartz veins in the Valley- and Ridge province and the anthracite fields of the Pennsylvania Appalachians. *Am. Mineral.* **76**, 320–340.

Klauda J. B., and Sandler S. I. (2002) Ab initio intermolecular potentials for gas hydrates and their predictions. *J. Phys. Chem. B* **106**(22), 5722–5732.

Konrad O., and Lankau T. (2005) Solubility of methane in water: the significance of the methane–water interaction potential. *J. Phys. Chem. B* **109**(49), 23596–23604.

Labotka T. C. (1991) Chemical and physical properties of fluids. *Rev. Mineral.* **26**, 43–104.

Lin F. (2005) Experimental Study of the PVTX Properties of the System H_2O–CH_4. Ph.D Thesis, Virginia Polytechnic Institute and State University.

Martyna G. J., Tobias D. J., and Klein M. L. (1994) Constant pressure molecular dynamics algorithms. *J. Chem. Phys.* **101**(5), 4177–4189.

Meinander N., and Tabisz G. C. (1983) The effect of the anisotropy of the intermolecular potential on the 2nd pressure virial-coefficient of CH_4. *J. Chem. Phys.* **79**(1), 416–421.

Michels A., and Nederbragt G. W. (1935) Isotherms of methane between 0 °C and 150 °C and densities 19 and 53 amagat (pressures between 20 and 80 atm). *Physica* **2**, 1000–1002.

Michels A., and Nederbragt G. W. (1936) Isotherms of methane between 0 and 150 °C for densities up to 225 amagat. Calculated specific heat, energy and entropy in the same region. *Physica* **3**, 569–577.

Mullis J., Dubessy J., Poty B., and O'Neil J. (1994) Fluid regimes during late stages of a continental collision: physical, chemical, and stable isotope measurements of fluid inclusions in fissure quartz from a geotraverse through the Central Alps, Switzerland. *Geochim. Cosmochim. Acta* **58**(10), 2239–2267.

Murad S., and Gubbins K. E. (1978) Molecular dynamics simulation of methane using a singularity-free algorithm. *Comput. Model. Matter*, 62–71.

Nagy J., Weaver D. F., and Smith V. H. (1995) A comprehensive study of alkane nonbonded empirical force-fields—suggestions for improved parameter sets. *J. Phys. Chem.* **99**(20), 8058–8065.

Olds R. H., Reamer H. H., Sage B. H., and Lacey W. N. (1943) Phase equilibrium in hydrocarbon systems:volumetric behavior of methane. *Ind. Eng. Chem. Res.* **35**, 922–924.

Righini R., Maki K., and Klein M. L. (1981) An intermolecular potential for methane. *Chem. Phys. Lett.* **80**(2), 301–305.

Robertso S. l., and Babb S. E. (1969) PVT properties of methane and propene to 10 kbar and 200 °C. *J. Chem. Phys.* **51**(4), 1357.

Roedder E. (1979) Fluid inclusions as samples of ore fluids. In *Geochemistry of Hydrothermal Ore Deposits* (ed. H. Barnes). Wiley-Interscience, pp. 684–737.

Roedder E. (1984) Fluid inclusions. In *Reviews in Mineralogy*, vol. 12. Mineralogical Society of America.

Ross M., and Ree F. H. (1980) Repulsive forces of simple molecules and mixtures at high-density and temperature. *J. Chem. Phys.* **73**(12), 6146–6152.

Saager B., and Fischer J. (1990) Predictive power of effective intermolecular pair potentials: MD simulation results for methane up to 1000 MPa. *Fluid Phase Equilibr.* **57**(1-2), 35–46.

Schamp H. W., Mason E. A., Richardson A. C. B., and Altman A. (1958) Compressibility and intermolecular forces in gases: methane. *Phys. Fluid* **1**, 329–337.

Schindler H., Vogelsang R., Staemmler V., Siddiqi M. A., and Svejda (1993) Ab initio intermolecular potentials of methane, nitrogen and methane+nitrogen and their use in Monte Carlo simulations of fluids and fluid mixtures. *Mol. Phys.* **80**(6), 1413–1429.

Schmidt C., and Bodnar R. J. (2000) Synthetic fluid inclusions: XVI. PVTX properties in the system H_2O–NaCl–CO_2 at elevated temperatures, pressures, and salinities. *Geochim. Cosmochim. Acta*(64), 3853–3869.

Schoen M., Hoheisel C., and Beyer O. (1986) Liquid CH_4, liquid CF_4 and the partially miscible liquid mixture CH_4/CF_4. A molecular dynamics study based on both a spherically symmetric and a four-centre Lennard–Jones potential model. *Mol. Phys.* **58**(4), 699–709.

Scott H. P., Hemley R. J., Mao H.-k., Herschbach D. R., Fried L. M., Howard W. M., and Bastea S. (2004) Generation of methane in the Earth's mantle: In situ high pressure–temperature measurements of carbonate reduction. *Proc. Natl. Acad. Sci. USA* **101**(39), 14023–14026.

Shmonov V. M., Sadus R. J., and Franck E. U. (1993) High-pressure phase-equilibria and supercritical PVT data of the binary water plus methane mixture to 723 K and 200 Mpa. *J. Phys. Chem.* **97**(35), 9054–9059.

Sretenskaya N. G., Zhakirov I. V., Shmonov V. M., and Shmulovich K. I. (1986) *Vodosoderzhaschie Fluidnye Systemy (Water-bearing Fluid Systems)*. Nauka Publishing House.

Stassen H. (1999) On the pair potential in dense fluid methane. *J. Mol.r Struct. Theochem* **464**(1-3), 107–119.

Strauss G., Bassen A., Zweier H., Bertagnolli H., Todheide K., Soper A. K., and Turner J. (1996) High-pressure neutron diffraction on fluid methane. *Phys. Rev. E* **53**(4), 3505–3517.

Sun R., and Duan Z. (2005) Prediction of CH_4 and CO_2 hydrate phase equilibrium and cage occupancy from ab initio intermolecular potentials. *Geochim. Cosmochim. Acta* **69**(18), 4411–4424.

Szczesniak M. M., Chalasinski G., Cybulski S. M., and Cieplak P. (1993) Abinitio study of the potential-energy surface of CH_4–H_2O. *J. Chem. Phys.* **98**(4), 3078–3089.

Trappeniers N. J., Wassenaar T., and Abels J. C. (1979) Isotherms and thermodynamic properties of methane at temperatures between 0 °C and 150 °C and at densities up to 570 amagat. *Phys. A* **98**(1–2), 289–297.

Tsiklis D. S., Linshits L. R., and Tsimmerman S. S. (1971) Molar volumes and thermodynamic properties of methane at high pressures and temperatures. *Dokl. Akad. Nuuk SSSR* **198**, 423–425.

Veto I., Futo I., Horvath I., and Szanto Z. (2004) Late and deep fermentative methanogenesis as reflected in the H–C–O–S isotopy of the methane-water system in deep aquifers of the Pannonian Basin (SE Hungary). *Org. Geochem.* **35**(6), 713–723.

Wagner W., and Prub A. (2002) The IAPWS formulation 1995 for the thermodynamic properties of ordinary water substance for general and scientific use. *J. Phys. Chem. Ref. Data* **31**(2), 387–535.

Wasserman E., Wood B., and Brodholt J. (1995) The static dielectric-constant of water at pressures up to 20 kbar and temperatures to 1273 K—experiment, simulations, and empirical equations. *Geochim. Cosmochim. Acta* **59**(1), 1–6.

Welsch (1973) Die system xenon-wasser und methan-wasser beiholen drticken und temperaturen. Ph.D thesis, University of Karlsruhe.

Williams D. E. (1967) Nonbonded potential parameters derived from crystalline hydrocarbons. *J. Chem. Phys.* **47**(11), 4680.

Zhang Z. G., and Duan Z. H. (2002) Phase equilibria of the system methane–ethane from temperature scaling Gibbs ensemble Monte Carlo simulation. *Geochim. Cosmochim. Acta* **66**(19), 3431–3439.

Zhang Z. G., and Duan Z. H. (2005) Prediction of the PVT properties of water over wide range of temperatures and pressures from molecular dynamics simulation. *Phys. Earth Planet. Inter.* **149**(3-4), 335–354.

Associate editor: James R. Rustad